

Technische Universität Dresden

Fakultät Umweltwissenschaften

Numerical analysis of thermo-hydro-mechanical (THM) processes in the clay based material

Dissertation zur Erlangung des akademischen Grades

Doctor-Ingenieur (Dr.-Ing.)

vorgelegt von

M.Sc. Xuerui Wang

geboren am 24. August 1987 in Sichuan, China

Gutachter:

Prof. Dr.-Ing. habil. Olaf Kolditz, Helmholtz-zentrum für Umweltforschung UFZ und Technische Universität Dresden

Prof. Dr.-Ing. habil. Michael Zhengmeng Hou, Technische Universität Clausthal

Prof. Xujin Zhang, Southwestern Research Institute of Water Transportation Engineering und Chongqing Jiaotong Universität

Tag der Verteidigung: 06. Oktober 2016

Erklärung zur Eröffnung des Promotionsverfahrens

1. Hiermit versichere ich, dass ich die vorliegende Arbeit ohne unzulässige Hilfe Dritter und ohne Benutzung anderer als der angegebenen Hilfsmittel angefertigt habe; die aus fremden Quellen direkt oder indirekt übernommenen Gedanken sind als solche kenntlich gemacht.
2. Bei der Auswahl und Auswertung des Materials sowie bei der Herstellung des Manuskripts habe ich Unterstützungsleistungen insbesondere bei der Anfertigung der Publikationen erhalten, die Bestandteil dieser kumulativen Dissertation sind. Diese Publikationen, sowie der jeweilige Anteil meiner eigenen Arbeit, sind in einer gesonderten Tabelle aufgelistet.
3. Weitere Personen waren an der geistigen Herstellung der vorliegenden Arbeit nicht beteiligt. Insbesondere habe ich nicht die Hilfe eines kommerziellen Promotionsberaters in Anspruch genommen. Dritte haben von mir weder unmittelbar noch mittelbar geldwerte Leistungen für Arbeiten erhalten, die im Zusammenhang mit dem Inhalt der vorgelegten Dissertation stehen.
4. Die Arbeit wurde bisher weder im Inland noch im Ausland in gleicher oder ähnlicher Form einer anderen Prüfungsbehörde vorgelegt und ist – sofern es sich nicht um eine kumulative Dissertation handelt – auch noch nicht veröffentlicht worden.
5. Sofern es sich um eine kumulative Dissertation gemäß § 10 Abs. 2 handelt, versichere ich die Einhaltung der dort genannten Bedingungen.
6. Ich bestätige, dass ich die Promotionsordnung der Fakultät Umweltwissenschaften der Technischen Universität Dresden anerkenne.

Hannover, 16.03.2016

Xuerui Wang

Abstract

Clay formations are investigated worldwide as potential host rock for the deep geological disposal of high-level radioactive waste (HLW). Usually bentonite is preferred as the buffer and backfill material in the disposal system. In the disposal of HLW, heat emission is one of the most important issues as it can generate a series of complex thermo-hydro-mechanical (THM) processes in the surrounding materials and thus change the material properties. In the context of safety assessment, it is important to understand the thermally induced THM interactions and the associated change in material properties. In this work, the thermally induced coupled THM behaviours in the clay host rock and in the bentonite buffer as well as the corresponding coupling effects among the relevant material properties are numerically analysed.

A coupled non-isothermal Richards flow mechanical model and a non-isothermal multiphase flow model were developed based on the scientific computer codes OpenGeoSys (OGS). Heat transfer in the porous media is governed by thermal conduction and advective flow of the pore fluids. Within the hydraulic processes, evaporation, vapour diffusion, and the unsaturated flow field are considered. Darcy's law is used to describe the advective flux of gas and liquid phases. The relative permeability of each phase is considered. The elastic deformation process is modelled by the generalized Hooke's law complemented with additional strain caused by swelling/shrinkage behaviour and by temperature change. In this study, special attention has been paid to the analysis of the thermally induced changes in material properties. The strong mechanical and hydraulic anisotropic properties of clay rock are described by a transversely isotropic mechanical model and by a transversely isotropic permeability tensor, respectively. The thermal anisotropy is described by adoption of the bedding-orientation-dependent thermal conductivity. The dependency of the thermal conductivity on the degree of water saturation, the dependency of the thermal effects on the water retention behaviour, and the dependency of the effects of the pore pressure variation on the permeability and the anisotropic swelling/shrinkage behaviour have been intensively analysed and the corresponding numerical models to consider those coupling effects have been developed.

The developed numerical model has been applied to simulate the laboratory and in situ heating experiments on the bentonite and clay rock at different scales. Firstly the laboratory heating experiment on Callovo-Oxfordian Clay (COX) and the laboratory long-term heating and hydration experiment on MX80 pellets were simulated. Based on the knowledge from the numerical analysis of the laboratory experiments, a 1:2 scale in situ heating experiment of an integrated system of the bentonite engineered barrier system (EBS) in the Opalinus Clay host rock was simulated. All the relevant operation phases were considered in the modelling. Besides, the modelling was extended to 50 years after the heat shut-down with the aim of predicting the long-term behaviours. Additionally, variation calculations were carried out to investigate the effects of the storage capacity of the Opalinus Clay on the thermally induced hydraulic response. In the long-term modelling, the effects of different saturated water permeabilities of buffer material on the resaturation process were analysed.

Based on the current researches and model developments, the observed THM behaviours of the bentonite buffer and the clay rock, that is, the measured evolution of temperature, pore pressure, humidity, swelling pressure, and so on in the laboratory and in situ experiments can be reproduced and interpreted well. It is proved that by using both a non-isothermal multiphase flow model and a non-isothermal Richards flow model combined with the corresponding thermal and mechanical models, the major THM behaviours can be captured. It is validated that the developed model is able to simulate the relevant coupled THM behaviours of clayey material under the well-defined laboratory conditions as well as under the complex natural disposal conditions.

Zusammenfassung

Wärmeausstrahlung ist eines der wichtigsten Themenfelder in der Endlagerung hoch radioaktiver Abfälle (HLW). Die Wärmeentwicklung kann in den umgebenden Materialien eine Reihe von komplexen thermo-hydro-mechanischen (THM) Prozessen verursachen und auch die Materialeigenschaften verändern. Dadurch kann die Integrität der Barriere beeinflusst werden. In dieser Arbeit wird das thermisch induzierte gekoppelte THM Verhalten im Tonstein und in der Bentonitverfüllung sowie im Übergangsbereich beider Materialien numerisch analysiert.

Das gekoppelte nicht-isotherme Multiphase Flow mechanische Modell und das nicht-isotherme Richards Flow mechanische Modell wurden mit Hilfe des Codes OpenGeoSys (OGS) entwickelt. Wärmeübertragung im porösen Medium findet über Wärmeleitung und advective Strömung des Porenfluides statt. Die Wärmeleitung wird durch das Fourier Gesetz beschrieben. In dem Modell sind die hydraulischen Prozesse Verdunstung, Dampf-Diffusion und die ungesättigte Zone berücksichtigt. Das Darcy-Gesetz wird unter Berücksichtigung der relativen Permeabilität der im Porenraum vorhandenen Phasen für den Strömungsprozess der flüssigen und gasförmigen Phasen angewandt. Der elastische Deformationsprozess wird durch das verallgemeinerte Hookesche Gesetz beschrieben, welches um die durch Temperaturänderung und durch Quellen bzw. Schrumpfen verursachte Verzerrung ergänzt wurde. In der vorliegenden Arbeit findet die Analyse der Materialeigenschaften im Zusammenhang mit dem Kopplungseffekt besondere Beachtung. Die starken anisotropen Eigenschaften des Opalinustons werden von einem transversal isotropen mechanischen Modell und dem Permeabilitätstensor dargestellt. Die thermische Anisotropie wird durch die von der Orientierung der Schichtung abhängige Wärmeleitfähigkeit beschrieben. Die Abhängigkeit zwischen Wärmeleitfähigkeit und Sättigungsgrad, der Einfluss der Temperatureffekte auf die Beziehung zwischen Kapillardruck und Wassersättigungsgrad und die Abhängigkeit der hydraulischen Permeabilität vom Schrumpf- und Quellverhalten sowie vom Porendruck wurden intensiv analysiert.

Das entwickelte numerische Modell wurde zur Simulation von Labor- und In-situ-Versuchen in unterschiedlichen Maßstäben verwendet. Zuerst wurden die im Labor durchgeführten Heiz-Experimente für den Callovo-Oxfordian Ton (COX) und das Langzeit-Heiz- und Aufsättigungs-Experiment für die MX80 Bentonit Pellets simuliert. Danach wurde auf Basis der Simulationsergebnisse und -erkenntnisse das im Felslabor Mont Terri im Maßstab 1:2 durchgeführte Heiz-Experiment HE-E modelliert. Im HE-E Experiment wird ein integriertes Barriersystem aus Bentonit (EBS - Engineered Barrier System) und dem Wirtsgestein Opalinuston untersucht. Die unterschiedlichen Betriebsphasen des HE-E Experimentes wurden ebenso berücksichtigt wie die Vorausberechnung des langfristigen Verhaltens. Dazu wurden die Berechnungen bis zu einem Zeitpunkt 50 Jahre nach Abschaltung des Erhitzers durchgeführt. Bei der HE-E Modellierung wurden Variationsrechnungen zur Untersuchung der Einflüsse der Speicherkapazität der Tonsteine auf die thermisch induzierten hydraulischen Reaktionen durchgeführt. Weiterhin wurden in die Vorausberechnung die Beziehung zwischen der wassergesättigten Permeabilität von Puffermaterialien und die benötigte Zeit für das Erreichen des vollgesättigten Zustandes untersucht.

Basierend auf aktuellen Kenntnissen kann das betrachtete Verhalten von Bentonit und Tonsteinen, z. B. die Entwicklung der Temperatur und des hydraulischen Drucks, in Labor- und Feldversuchen gut reproduziert und interpretiert werden. Es wurde nachgewiesen, dass mit der Anwendung von nicht-isothermen Multiphase Flow Modellen und nicht-isothermen Richards Flow Modellen in Kombination mit entsprechenden thermischen und mechanischen Modellen die meisten wichtigsten THM-Prozesse erfasst werden können. Das entwickelte Modell kann in weiteren Untersuchungen zu gekoppelten THM-Prozessen und thermisch induzierten Änderungen der Materialeigenschaften sowohl unter gut definierten Laborbedingungen, als auch unter den komplexen natürlichen Bedingungen eines Endlagers für hoch radioaktive Abfälle angewendet werden.

Acknowledgments

Firstly, I am extremely grateful to my supervisor Prof. Olaf Kolditz, the head of the Department of Environment Informatics in the Helmholtz Centre for Environmental Research (UFZ) for the continuous support and guidance of my Ph.D study and the related researches and for his patience, motivation, and encouragement. His recommendations and instructions have enabled me to assemble and finish the dissertation effectively.

I would like to express my sincere gratitude to Prof. Michael Zhengmeng Hou at Technical University Clausthal, who is one of the co-referees of my thesis. He has supported and encouraged me throughout my academic career and given me valuable comments on my research. I would also like to thank the rest of co-referees of my thesis: Prof. Zhang, at Chongqing Jiaotong University for his insightful comments and encouragement, but also for the hard question which incited me to widen my research from various perspectives.

My sincere thanks also goes to my mentor Dr. –Ing. Hua Shao at German Federal Institute for Geoscience and Natural Resource (BGR) who have guided, encouraged and supported me throughout the research process. Without his help it would not be possible to conduct this research.

I would like to thank the colleagues at BGR who have given me help and advices. In particular, I want to thank Dr.-Ing. Jürgen Hesser for his support of my research and for his precious suggestions and advices especially in rock mechanics issues. Also, I want to thank Herbert Kunz for the development of the pre-post program GINA and his guidance about using GINA to generate model mesh and evaluate data. Besides, I would like to express my thanks to Benjamin Paul, who has helped me to improve the language aspect of this dissertation.

I want to express my thanks to Dr. Wenqing Wang at UFZ for his immense knowledge and continuous support of my research. He has helped me a lot in the understanding and developing of the numerical program OpenGeoSys. I also would like to thank Dr. –Ing Wenjie Xu at the Zhejiang University for enlightening me the first glance of this research and the continuous help.

I would like to thank my parents who always support, encourage me throughout the course of this dissertations and my life in general. This last word of acknowledgment I have saved for my husband, Shuang Chen, without whom this effort would have been worth nothing. Your love, support and constant patience have taught me so much about sacrifice, discipline and compromise.

Hannover, 16.03.2016

Xuerui Wang

Content

1. Introduction.....	1
1.1 Motivation and objectives.....	1
1.2 State of the art	2
1.3 Dissertation structure.....	4
2. Mathematical and numerical models.....	4
2.1 Balance equations	4
2.2 Constitutive equations	5
2.2.1 Thermal model	5
2.2.2 Hydraulic model.....	6
2.2.3 Mechanical model	10
2.3 Numerical approaching to the relevant coupling effects.....	11
2.3.1 Pore pressure dependent permeability model	11
2.3.2 Saturation dependent thermal conductivity model.....	12
2.3.3 Modified van Genuchten function	13
2.3.4 Swelling and shrinkage behaviour.....	14
3 Model validation and interpretation.....	15
3.1 Modelling of the laboratory heating experiment on COX.....	15
3.1.1 Experiment description	15
3.1.2 Model set up.....	16
3.1.3 Results analysis.....	17
3.2 Modelling of the laboratory column test on the granular MX80 bentonite	18
3.2.1 Experiment description	18
3.2.2 Model set up.....	19
3.2.3 Results analysis.....	20
3.3 Modelling of the HE-E in situ heating experiment	23
3.3.1 Experiment description	23
3.3.2 Model features	24
3.3.3 Results analysis.....	25
4. Conclusions and outlook	29
Reference	i
List of publications.....	iv
Theses.....	v
Thesen	vi

1. Introduction

1.1 Motivation and objectives

Heat emission is one of the most important issues in the disposal of high-level radioactive waste (HLW) during the early closure phase. Generally the change of temperature can induce complex interactions among the thermal, hydraulic, and mechanical (THM) fields (Fig. 1, left). Thermal loading can induce expansion of pore fluids and solid skeleton and change the pore space, which leads to the increase of pore pressure. Furthermore, the increase of temperature can cause a decrease of gas and liquid viscosity ($T \gg H$). It can also induce deformation with stress variations ($T \gg M$). On the other hand, the change of pore pressure has an effect on the effective stress ($H \gg M$) and the degree of water saturation. The water/gas flow can influence the heat conductivity ($H \gg T$) because of the saturation-dependent thermal conductivity [EP1]. Additionally, the pore pressure change can change the pore space structure, and the surface tension at the grain and water interface can also be changed due to the temperature change. The changes of both the pore space structure and the surface tension have impacts on the water retention behaviour.

With respect to the different operation phases of one disposal of HLW, firstly the tunnel excavation could change the saturation distribution around the tunnel wall and thereby affect the later heating transfer and evolution of pore pressure in the host rock close to the tunnel. Besides, in the excavation damage zone (EDZ), an enhanced hydraulic conductivity is also expected. During the early closure phase, heat flux emitted from the HLW will be conducted by different species of the porous medium and advected by liquid and gas flux into the surrounding material, causing a series of coupled THM processes (Fig. 1, right). In EBS, a desaturation process will take place, firstly due to the evaporation of water caused by the high temperature. Meanwhile, a vapour gradient will be generated within the material which can drive vapour flow from the warm area to the cold area, and consequently the distribution of humidity will be changed. The change in saturation can in turn result in a change of the thermal conductivity and thus affect the heat transfer process. Under the above processes, local micro-fissures may be generated due to the shrinkage behaviour and stress redistribution, which can lead to an increase of the hydraulic conductivity. Afterwards, with the dissipation of the heat, the temperature will decrease in the buffer material. Then a resaturation process will take place due to the water intake from the host rock into the buffer material. The local micro-fissures generated during the desaturation process can be sealed due to the swelling behaviour during the resaturation process. In host rock, when compacted clay is subject to heating, a strong hydraulic response can be induced. A pore pressure rise will generally result from the thermal expansion of solid, water, and gas, and the increase of pore pressure could be very large and could reach hydraulic fracture conditions. Also, the thermally induced strain and the variation in pore pressure can change the stress state. Afterwards, the overpressure will dissipate and the consolidation process will take place [EP3].

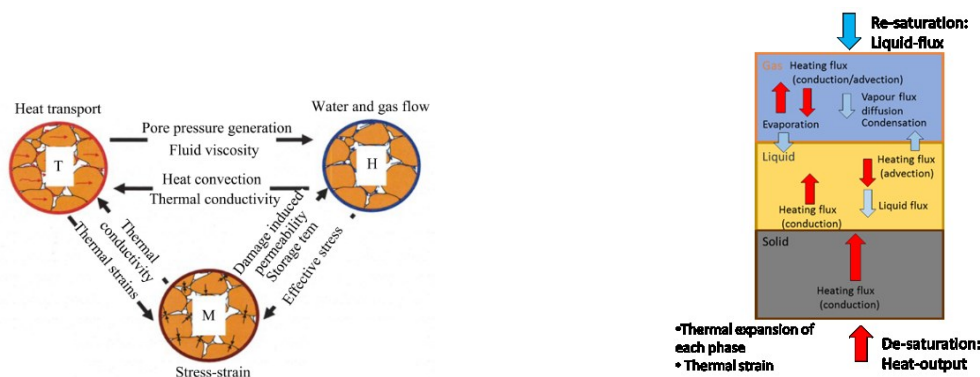


Fig. 1: Overview of thermally induced THM interactions in porous media (left: Gens et al., 2007) and possible coupled THM processes in bentonite EBS (right)

This thesis focuses on the development and application of numerical modelling for a better understanding of the thermally induced coupled THM processes in the bentonite EBS and in the clay host rock with respect to the disposal of HLW and, thereby, the analysis of the thermal effects on the safety-relevant parameters (e.g. hydraulic conductivity, water retention behaviour, swelling behaviour, and pore pressure evolution). A non-isothermal multiphase flow, thermal, mechanical coupled model and a non-isothermal Richards flow, thermal, mechanical coupled model have been developed and applied to simulate the heating experiments on the clayey materials. The experimental observations were successfully reproduced and interpreted in the modelling.

1.2 State of the art

In the last two decades, highly consolidated clay formations have been investigated worldwide as potential host rock for deep geological disposal of HLW due to their favourable properties such as very low hydraulic permeability, predominant diffusive mass transport, good isolation capability, homogeneous structure, and especially high sorption capacity for most radionuclides, as well as the ability to seal cracks and fissure by swelling. To confirm the safety functions of the repository in clay host rock and to understand the thermally induced coupled THM processes and change of material properties, many heating experiments at different scales have been performed in situ and in laboratories: that is, the ATLAS experiment on the Boom Clay in the rock laboratory at Mol in Belgium (De Bruyn and Labat, 2002), the TER experiment on the Callovo-Oxfordian (COX) Clay at Bure site in France (Wileveau and Su, 2007), and the HE-D experiment on the Opalinus Clay at Mont Terri underground research laboratory in Switzerland (Wileveau, 2005; Zhang et al., 2009). In a commonly designed disposal of HLW, bentonite is preferred as buffer and backfill material in the EBS due to the low thermal conductivity, low permeability, swelling capacity, and retention properties. As buffer material, bentonite is filled between canisters and surrounding rock. Thus in the operation of the nuclear waste repository, the bentonite is expected to experience the maximum temperature in the early post-closure phase (Villar, 2002), when it will vary between 90 and 150° C (Johnson et al., 2002) depending on the repository concept. At such high temperatures, strong coupled THM processes can be generated. To demonstrate the feasibility of using bentonite as a buffer material in the different repository concepts and to determine the strongly coupled THM behaviours, many in situ experiments have been carried out in underground rock laboratories (URLs). The first long-term full-scale experiment was the Full-scale Engineered Barriers EXperiment (FEBEX) in the granitic rock at the

Grimsel Test Site in Switzerland (Huertas et al., 2000), in which compacted Ca-bentonite was tested under a thermal loading of 100 °C for over 15 years. Similarly, the Prototype Repository experiment on the MX80 Na-bentonite was carried out in the Äspö Rock Laboratory in Sweden (Andersson et al., 2005). To complement the in situ experiments, numerous small-scale and mock-up-scale experiments under well-defined laboratory conditions have been carried out. For example, the FEBEX mock-up test conducted by CIEMAT (Centro de Investigaciones Energéticas, Medioambientales y Tecnológicas) (ENRESA, 2000) simulated the long-term Ca-bentonite behaviour at a temperature of 100 °C as a comparable experimental setup to the in situ FEBEX experiment at the Grimsel test site, which is however, under well-defined boundary conditions and without rock heterogeneity. A series of tests aiming to determine the THM properties of MX80 used in the Prototype Repository have been conducted by Clay Technology, Sweden (Andersson et al., 2005). In the Swiss concept for a repository of HLW, the Opalinus Clay and MX80 bentonite are considered as potential host rock and buffer material in the EBS respectively. The temperature of the canister surface is estimated to be up to 140 °C owing to the heat emission from the HLW. However, so far only a few large-scale field tests have been carried out to evaluate the detailed behaviours of the integrated bentonite EBS in clay host rock in response to high temperatures of up to 140 °C at the canister surface (Gaus et al., 2014). For these, a Full-Scale Emplacement (FE) experiment at Mont Terri URL in Switzerland is being constructed to simulate the long-term coupled THM behaviour and to study the interaction between the buffer material MX80 and the saturated Opalinus Clay formation under in situ conditions (Müller et al., 2012). Similarly, a 1:2 scale heating experiment (HE-E) constructed with two independent heating sections has been in operation in the Opalinus Clay at the Mont Terri URL. One section is filled with granular MX80 and the other with sand–bentonite mixture. To complement the HE-E experiment, CIEMAT has been performing a long-term laboratory heating and hydration test on MX80 and sand–bentonite pellets since 2012. The numerous experiments have provided an extensive database for the numerical analyses.

Recently, numerical modelling has become a more and more important instrument to analyse the THM coupled processes in porous and fractured media. The concept of the numerical analysis of the coupled processes in geo-systems has been studied and presented in many former researches (Stephansson et al., 2004; Kolditz et al., 2012). It has been confirmed that numerical models can be used in different geotechnical applications, for instance disposal of nuclear waste, geothermal engineering, storage of CO₂, and so on. To advance the understanding and modelling of the complex THM(C) processes in geo-systems, the international research project DECOVALEX (DEvelopment of COupled models and their VALidation against EXperiments) (Hudson and Jing, 2013) has been conducted since 1992. In the recent phase, DECOVALEX 2015 (2012–2015), one of the tasks is geared towards the understanding of THM processes in a bentonite buffer and clayey host rock by means of development of numerical models. The task is approached stepwise by modelling of 1) the HE-D in situ heating test, 2) a laboratory column test on bentonite pellets, and 3) the HE-E in situ heating test. In the first two steps, the material properties of clay host rock and bentonite buffer material have been intensively analysed. The current step is the modelling of the HE-E test (integrating buffer materials and host rock), which is based on knowledge from the modelling of the HE-D test and the column test. The experimental observations have been numerically analysed by eight modelling teams using different codes and different numerical methods. In this dissertation, the presented modelling

work of the laboratory column test on MX80 bentonite [EP2] and the HE-E test [EP3] are involved in the DECOVALEX project.

So far, only a few experimental and numerical works have considered the integrated disposal system of EBS in the host rock. Most of the previous works focused on estimation of the behaviours of one material (buffer or host rock) with respect to one operation phase. In this work, the integrated disposal system of EBS and host rock is numerically simulated based on a large experimental database. The properties of the material are intensively studied, including the strong thermal, hydraulic, and mechanic anisotropy of clay rock, the swelling behaviour of bentonite and clay, the coupling effects from the water saturation on the thermal conductivity, the temperature effects on water retention behaviour, the sensibility of variation of storage capacity on the pore pressure evolution, and the effects of permeability of buffer material on the resaturation process. Furthermore, not only the heat emission phase but also the excavation, ventilation, and emplacement of buffer-induced HM behaviour and change of host rock properties is simulated, and in this way their effects on the coupled behaviours during the later heating phase can be captured.

1.3 Dissertation structure

This thesis is structured in four chapters. In the first Chapter the backgrounds and the motivations of this PhD study are introduced. In Chapter 2 the theoretical backgrounds, the general mathematical formulations and the developed numerical approaching to solve the presented coupled THM problems are described. Chapter 3 demonstrates the simulations of three heating experiments on clay based material using the developed numerical models and the results analysis. In Chapter 4 summary of this work and some outlooks for the future investigations are given. At the end of the thesis the publications produced by this work are listed.

2. Mathematical and numerical models

2.1 Balance equations

To analyse the THM coupling processes, the porous medium is usually assumed as a homogenous continuum, which are composed of three species: mineral, water and gas distributed as three phases: solid, liquid and gas. The liquid phase contains water and dissolved air, while the gas phase is a mixture of dry air and vapour. Generally, for numerical analysis of the coupled THM processes a set of balance equations for internal energy, solid (s) mass, water (w) mass, gas (g) mass and stress equilibrium has to be solved (Booker and Savvidou, 1985; Olivella et al., 1994):

Solid mass balance:

$$\frac{\partial}{\partial t}(\rho^s(1-\phi)) + \nabla \cdot \mathbf{J}^s = q^s \quad (1)$$

where ρ^s is solid density, ϕ is porosity, \mathbf{J}^s is the flux of solid, and q^s is external mass supply of solid per unit volume of medium

Water mass balance:

$$\frac{\partial}{\partial t}(\rho_w^l S^l \phi + \rho_w^g S^g \phi) + \nabla \cdot (\mathbf{J}_w^l + \mathbf{J}_w^g) = q_w \quad (2)$$

where ρ_w^l and ρ_w^g are respectively the mass fraction of water in liquid phase and gas phase. S^l and S^g are respectively the volumetric fraction of liquid and gas with respect to the pore volume. \mathbf{J}_w^l and \mathbf{J}_w^g denote respectively the total mass flux of water in the liquid and gas phases with respect to a fixed reference system. q_w is the external mass supply of water per unit volume of medium.

Air mass balance:

$$\frac{\partial}{\partial t}(\rho_a^l S^l + \rho_a^g S^g) + \nabla \cdot (\mathbf{J}_a^l + \mathbf{J}_a^g) = q_a \quad (3)$$

where ρ_a^l and ρ_a^g are respectively the mass of dry air per unit volume of liquid phase and gas phase. \mathbf{J}_a^l and \mathbf{J}_a^g denote respectively the total mass flux of air in the liquid and gas phases with respect to a fixed reference system. q_a is the external mass supply of air per unit volume of medium.

Internal energy balance:

$$\frac{\partial}{\partial t}[E^s \rho^s (1 - \phi) + E^l \rho^l S^l \phi + E^g \rho^g S^g \phi] + \nabla \cdot (i_c + \mathbf{J}^{Es} + \mathbf{J}^{El} + \mathbf{J}^{Eg}) = q^E \quad (4)$$

where E^s , E^l , E^g are respectively the specific internal energies of the solid, liquid and gas phases. ρ^l and ρ^g are the density of the liquid and gas. i_c is the conductive heat flux and \mathbf{J}^{Es} , \mathbf{J}^{El} , \mathbf{J}^{Eg} are respectively the advective energy flux of each three phases with respect to a fixed reference system. q^E is external energy supply per unit volume of the medium.

Stress equilibrium:

$$\nabla \cdot \boldsymbol{\sigma} + \mathbf{b} = 0 \quad (5)$$

where $\boldsymbol{\sigma}$ is the total stress tensor, \mathbf{b} is the body forces vector.

2.2 Constitutive equations

2.2.1 Thermal model

Heat transfer in the porous media is governed by conduction and by advective flow of water, gas and vapour. Using Fourier's law to describe thermal conduction, the heat balance equation can be expressed as the simplification of the energy balance equation (Eq. (4)):

$$c\rho \frac{\partial T}{\partial t} + c\rho v \cdot \nabla T - \nabla(\lambda \cdot \nabla T) = q_{th} \quad (6)$$

Where ∇T is the temperature gradient, c is the heat specific capacity, ρ is the density, v is advection velocity and λ is the thermal conductivity of porous medium.

2.2 2. Hydraulic model

2.2.2.1 Non-isothermal multiphase flow model

In the non-isothermal multiphase model two phases γ : liquid ($\gamma = l$) and gas ($\gamma = g$) are considered.

And the total hydraulic flux \mathbf{J}_k^γ (Eqs. 2 and 3) contains two parts: the advective part \mathbf{J}_{Ak}^γ and the diffusion part \mathbf{J}_{Dk}^γ :

$$\mathbf{J}_k^\gamma = \mathbf{J}_{Ak}^\gamma + \mathbf{J}_{Dk}^\gamma \quad (7)$$

where k refers to different species in each phase where ($k = a$) for dry air, ($k = w$) for water.

The advective part is according to the Darcy's law and include liquid flux \mathbf{J}_{Ak}^l as well as gas flux \mathbf{J}_{Ak}^g :

$$\mathbf{J}_{Ak}^g = -\rho^g \cdot \frac{\mathbf{k} \cdot k_{rel}^g}{\mu^g} \cdot (\nabla p^g + \rho^g \cdot \mathbf{g}) \quad (8)$$

$$\mathbf{J}_{Ak}^l = -\rho^l \cdot \frac{\mathbf{k} \cdot k_{rel}^l}{\mu^l} \cdot (\nabla p^g - \nabla p^c + \rho^l \cdot \mathbf{g}) \quad (9)$$

where \mathbf{k} is the intrinsic permeability, k_{rel}^γ is the relative permeability of each phase, \mathbf{g} is the gravity acceleration, μ^γ is the viscosity.

The diffusion part is based on the Fick's law:

$$\mathbf{J}_{Dk}^\gamma = -\rho^\gamma \mathbf{D}_k^\gamma \nabla \left(\frac{\rho_k^\gamma}{\rho_\gamma} \right) \quad (10)$$

where \mathbf{D}_k^γ is the diffusion tensor and obviously $\mathbf{D}_w^l = 0$.

Within the context of phase change, only the vaporization will be considered, however the condensation processes are neglected [EP2]. Therefore, \mathbf{J}_a^l is assumed as 0. Diffusion is only observed in the binary gas phase and the corresponding diffusion part can be obtained as (Lewis and Schrefler, 1998):

$$\mathbf{J}_{Dk}^g = -\rho^g \frac{M_a M_w}{M_g^2} \mathbf{D}_k^g \nabla \left(\frac{p_k^g}{p^g} \right) \quad (11)$$

Here, p_k^g denotes the partial pressure induced by phase change, M is the molar mass, subscript a stands for dry gas, w for water and g for gas mixture. The molar mass of gas mixture M_g then can be written as:

$$\frac{1}{M_g} = \frac{1}{\rho_g} \left(\frac{\rho_w^g}{M_w} + \frac{\rho_a^g}{M_a} \right) \quad (12)$$

with the density of gas mixture ρ^g , the mass concentration of dry gas component ρ_a^g and the mass from water vapour component ρ_w^g in the gas phase. Since $\rho^g = \rho_a^g + \rho_w^g$, the binary diffusion of gas (dry air) and vapour are assumed as:

$$\mathbf{J}_{Dw}^g + \mathbf{J}_{Da}^g = 0 \quad (13)$$

under the physically appropriate assumption of $\mathbf{D}_a^g = \mathbf{D}_w^g = \mathbf{D}^g$

Considering the definition of flux vectors: Eqs. (7), (8), (9) and (11), since the capillary pressure $p^c = p^g - p^w$, the gas pressure p^g , displacement u and temperature T are chosen as a primary variables and under the assumption: $S^g = 1 - S^l$, the porous medium mass balance for the solid skeleton (Eq. (1)) combined with water and vapour (Eq. (2)) can be expanded as follows:

$$\begin{aligned} & \phi(\rho_w^l - \rho_w^g) \frac{\partial S^l}{\partial p^c} \frac{\partial p^c}{\partial t} + [S^l \rho_w^l + (1 - S^l) \rho_w^g] \nabla \cdot \mathbf{i} \\ & (1 - S^l) \phi \left(\frac{\partial \rho_w^g}{\partial T} \frac{\partial T}{\partial t} + \frac{\partial \rho_w^g}{\partial p^g} \frac{\partial p^g}{\partial t} + \frac{\partial \rho_w^g}{\partial p^c} \frac{\partial p^c}{\partial t} \right) \\ & - \nabla \cdot \left[\rho_w^l \frac{Kk_{rel}^l}{\mu^l} (\nabla(p^g - p^c) - \rho^l \mathbf{g}) \right] \\ & - \nabla \cdot \left[\rho_w^g \frac{Kk_{rel}^g}{\mu^g} (\nabla(p^g - \rho^g \mathbf{g})) \right] \\ & - \nabla \cdot \left[\rho^g \frac{M_a M_w}{M_g^2} \mathbf{D}^g \nabla \left(\frac{p_w^g}{p^g} \right) \right] = q_w \end{aligned} \quad (14)$$

Similarly, the extended mass balance equation for solid skeleton (Eq.(1)) and dry air (Eq. (3)) can be written as:

$$\begin{aligned}
& -\phi \rho_a^g \left(\frac{\partial S^l}{\partial T} \frac{\partial T}{\partial t} + \frac{\partial S^l}{\partial T} \frac{\partial p^c}{\partial t} \right) + [(1-S^w) \rho_a^g] \nabla_i \cdot \\
& (1-S^l) \phi \left(\frac{\partial \rho_a^g}{\partial T} \frac{\partial T}{\partial t} + \frac{\partial \rho_a^g}{\partial p^g} \frac{\partial p^g}{\partial t} + \frac{\partial \rho_a^g}{\partial p^c} \frac{\partial p^c}{\partial t} \right) \\
& -\nabla \cdot \left[\rho_a^g \frac{K k_{rel}^g}{\mu^l} (\nabla p^g - \rho^g \mathbf{g}) \right] \\
& -\nabla \cdot \left[\rho^g \frac{M_a M_w}{M_g^2} \mathbf{D}^g \nabla \left(\frac{p_a^g}{p^g} \right) \right] = q_a
\end{aligned} \tag{15}$$

In order to enhance the numerical stability, the gas phase density related derivative terms in the mass balance (Eqs. (14) and (15)) are expanded by the chain rule:

$$\nabla \left(\frac{p_a^g}{p^g} \right) = -\nabla \left(\frac{p_w^g}{p^g} \right) = \frac{p_w^g}{(p^g)^2} \nabla p^g - \frac{1}{p^g} \frac{\partial p_w^g}{\partial p^c} \nabla p^c - \frac{1}{p^g} \frac{\partial p_w^g}{\partial T} \nabla T \tag{16}$$

According to the Clapeyron equation for an ideal gas and Dalton's law holds:

$$\begin{aligned}
p_a^g &= \rho_a^g RT / M_a & p_w^g &= \rho_w^g RT / M_w \\
p^g &= p_a^g + p_w^g
\end{aligned} \tag{17}$$

where R is the universal gas constant with a value of 8.314 J/mol/K.

In the partially saturated zone, the equilibrium water vapour pressure is given by the Kelvin-Laplace equation:

$$p_w^g = p_{ws}^g \exp\left(-\frac{p^c M_w}{\rho_w^l RT}\right) \tag{18}$$

Thereby p_{ws}^g is the saturated vapour pressure as given in (Phillip and de Vries, 1957):

$$p_{ws}^g = 10^{-3} \exp(19.84 - 4975.9/T) \frac{RT}{M_w} \tag{19}$$

Based on Eq. (17), Eq. (16) can be further expanded as:

$$\nabla \left(\frac{p_a^g}{p^g} \right) = -\nabla \left(\frac{p_w^g}{p^g} \right) = \frac{p_w^g}{(p^g)^2} \nabla p^g + \frac{\rho_w^g}{p^g \rho_w^l} \nabla p^c - \frac{1}{p^g} \frac{\partial p_w^g}{\partial T} \nabla T \tag{20}$$

Eq. (20) presents the spatial variations of the mass transfer from liquid phase to gas phase (water evaporation) and also indicate how the changes of each variable-- p^g , p^c and T -- contribute to the mass transfer. It can also be seen that, besides the pressure gradient, thermal diffusion plays a role in the Laplacians term in the mass balance equations (Eqs. (14) and (15)).

2.2.2.2 Non-isothermal Richards flow model

In the Richards flow model the mobility of the gas in the porous medium is neglected with the assumption that gas pressure changes is very small (Wang et al., 2011). Gas pressure is assumed as constant and equal to the atmospheric pressure. Thus, the equation for the gas component (Eq. (15)) can be neglected. Instead of primary variable of gas pressure and capillary pressure in the multiphase flow model, in the Richards flow model water pressure is considered as primary variable. Thus the mass balance equation (Eq. (14)) can be simplified as:

$$\begin{aligned}
& \phi(\rho_w^l - \rho_w^g) \left(\frac{\partial S^l}{\partial T} \frac{\partial T}{\partial t} - \frac{\partial S^l}{\partial p^l} \frac{\partial p^l}{\partial t} \right) + [S^l \rho_w^l + (1 - S^l) \rho_w^g] \nabla i \\
& + (1 - S^l) \phi \left(\frac{\partial \rho_w^g}{\partial T} \frac{\partial T}{\partial t} - \frac{\partial \rho_w^g}{\partial p^l} \frac{\partial p^l}{\partial t} \right) \\
& - \nabla \cdot \left[\rho_w^l \frac{K k_{rel}^l}{\mu^l} \nabla (p^l - \rho^l g) \right] \\
& - \nabla \cdot \left[\rho_w^g \frac{M_a M_w}{M_g^2} \mathbf{D}_w^g \nabla \left(\frac{p_w^g}{p^g} \right) \right] = q_w
\end{aligned} \tag{21}$$

According to (Rutqvist et al, 2001) the diffusion term in Eq. (21) can be extended as:

$$\rho_w^g \frac{M_a M_w}{M_g^2} \mathbf{D}_w^g \nabla \left(\frac{p_w^g}{p^g} \right) \approx D_{pv} \nabla p^l + f_{Tv} D_{Tv} \nabla T \tag{22}$$

Where f_{Tv} represents an enhancement factor for the thermal diffusion term. The variables D_{pv} and D_{Tv} denote particular diffusion coefficient and given by:

$$D_{pv} = \frac{D_v \rho_w^g}{\rho_w^l R_v T} \tag{23}$$

$$D_{Tv} = D_v \left(RH \frac{\partial \rho_{vs}}{\partial T} - \frac{\rho_w^g p^l}{\rho_w^l R_v T^2} \right) \tag{24}$$

where $R_v = 461.5 \text{ J}/(\text{kg K})$ is the specific gas constant, D_v is the vapour diffusion coefficient, $RH = \exp(p^l / \rho_w^l R_v T)$ is the relative humidity, ρ_{vs} is the saturated vapour density, and can be given by an empirical function (Rutqvist et al. 2001):

$$\rho_{vs} = 10^{-3} \exp(19.891 - 4975 / T) \tag{25}$$

In both non-isothermal multiphase flow and non-isothermal Richards flow model, the well-known van Genuchten function is applied to describe the water retention behaviour:

$$p^c = p^0 \left[S_{eff}^{-1/m} - 1 \right]^{(1-m)} \tag{26}$$

Where p^0 is the air entry pressure, m is the dimensionless pore size distribution index. S_{eff} is the effective saturation, which can be calculated as:

$$S_{eff} = \frac{S - S_r}{S_{max} - S_r} \quad (27)$$

With S_{max} and S_r as the maximum and residual saturation.

2.2.3 Mechanical model

The mechanical properties are described by an elastic constitutive model based on the generalised Hooke's law and complemented with the thermally-induced strain and swelling-induced stress:

$$d\sigma_{ij} = \mathbf{D}_{ij}^e \cdot (d\varepsilon - d\varepsilon_T) - d\sigma_{sw} \quad (28)$$

where \mathbf{D}_{ij}^e is the elastic stiffness matrix, which can be determined by the Young's modulus E and the Poisson's ratio ν in the linear elasticity. $d\sigma_{sw}$ is additional stress increment caused by material swelling behaviour. $d\varepsilon$ is the total strain increment, $d\varepsilon_T$ is the additional strain caused by the temperature change, which is considered as an additional strain tensor in the mechanical model. It is related to the linear thermal expansion coefficient a and the temperature change:

$$d\varepsilon_T = adT \quad (29)$$

σ_{ij} is the effective stress and based on the Terzaghi's effective stress concept. Additionally, in unsaturated area, the effective stress concept is extended by Bishop's model:

$$\sigma_{ij} = \sigma_{tot} - \alpha p^w (S^w)^\chi \mathbf{I} \quad (30)$$

Where σ_{tot} is the total stress vector. α is the Biot coefficient, p^w is the pore pressure, S^w is water saturation, χ is constant model parameter, \mathbf{I} is the identity vector.

A transversely isotropic elastic model was developed to describe the strong anisotropic mechanical behaviour of the Clay rock:

$$\begin{bmatrix} \varepsilon_{11} \\ \varepsilon_{22} \\ \varepsilon_{33} \\ \varepsilon_{12} \\ \varepsilon_{13} \\ \varepsilon_{23} \end{bmatrix} = \begin{bmatrix} 1/E_1 & -\nu_{12}/E_2 & -\nu_{13}/E_3 \\ -\nu_{21}/E_1 & 1/E_2 & -\nu_{23}/E_3 \\ -\nu_{31}/E_1 & -\nu_{32}/E_1 & 1/E_3 \\ & & & 1/2G_{12} \\ & & & & 1/2G_{13} \\ & & & & & 1/2G_{23} \end{bmatrix} \begin{bmatrix} \sigma_{11} \\ \sigma_{22} \\ \sigma_{33} \\ \sigma_{12} \\ \sigma_{13} \\ \sigma_{23} \end{bmatrix} \quad (31)$$

where $E_1 = E_2 = E_{\parallel}$ are Young's modulus in the bedding plane. $E_3 = E_{\perp}$ is Young's modulus in the direction normal to the bedding plane. $G_{12} = G_{13} = G_{\parallel}$ are the shear modulus parallel to bedding, and $G_{23} = G_{\perp}$ is shear modulus normal to the bedding plane. $\nu_{12} = \nu_{21} = \nu_{\parallel}$ are poisson's ration in the bedding plane. $\nu_{13} = \nu_{23} = \nu_{\parallel}$ and $\nu_{32} = \nu_{31} = \nu_{\perp}$ are poisson's ratio in the anisotropic direction. ε_{ij} is the total strain.

2.3 Numerical approaching to the relevant coupling effects

According to the experimental data base and the experimental observations several numerical approaches were developed to extend the understanding of the coupling effects among the relevant material parameters.

2.3.1 Pore pressure dependent permeability model

When the saturated clay is subjected to thermal loading, strong pore pressure will be induced due to the thermal expansion of solid and pore fluids. Under the strong pore pressure response the pore structure could be changed. Generally, the increase of pore pressure could enlarge the pore space thus lead to the increase of the hydraulic permeability. Backwards, the hydraulic permeability has a significant impact on the pore pressure evolution. If the change of the pore space are within the elastic range, with the decrease of the pore pressure, the pore space will regress. Herewith the increased permeability could be reduced until to the initial level. The above mentioned coupled phenomenon have been proved by some former researches (e. g. Kozeny, 1927; Ghabezloo, 2010) and have also been observed in many laboratory and in situ experiments that were theoretically and numerically investigated (e.g. Walls, 1982; Li et al., 2009; Xu et al., 2011; Xu et al., 2013). Xu et al. (2011) had proposed a linear relationship between permeability change and gas pressure in the pore space, with the following two assumptions: (1) Relative low pore pressure can only cause extension or compaction of pore space that has limited effects on permeability; (2) If gas pressure oversteps a threshold value (e.g. the minimal principal stress), micro- or macro-fractures can be generated which can cause a significant permeability increase. The permeability is assumed to increase slightly if gas pressure is lower than this threshold. Otherwise the permeability increases rapidly after the gas pressure exceeds the threshold. Based on these assumptions, a pore pressure dependent permeability (Eq. (32)) was developed and implemented. It is assumed in the model that the permeability begins to increase if the pore pressure is higher than a critical value:

$$k = \beta k^{\text{int}} \quad (32)$$

where k^{int} is the initial permeability. β is the empirical permeability enhancement factor and can be determined by a linear function shown in Fig. 2. p_{cri} is the assumed critical pore pressure which is determined by using the trial and error method.

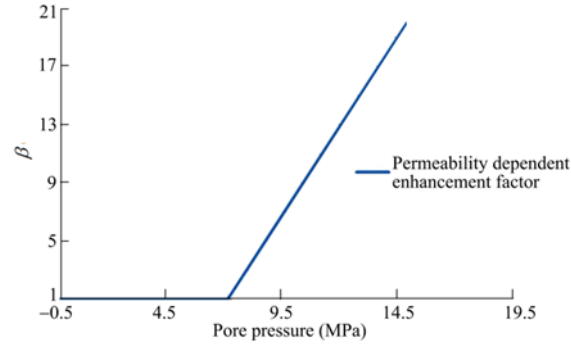


Fig. 2: Permeability enhancement factor as a function of pore pressure.

The validity of the proposed model is still not proven for a general application because the in model described change of the pore space is assumed within the elastic range.

2.3.2 Saturation dependent thermal conductivity model

Many laboratory experiments (Börgesson et al. 1994, Kahr and Müller-Vonmoos 1982 and Villar 2002) have verified that the thermal conductivity can be strongly affected by the degree of water saturation. A function to describe the dependence of the thermal conductivity on water saturation was developed and implemented based on the study in (Åkesson et al., 2010):

$$\lambda(S_r) = \lambda_{sat}^{S^l} \lambda_{dry}^{(1-S^l)} \quad (33)$$

where λ_{sat} is the thermal conductivity of saturated sample, λ_{dry} is the thermal conductivity of dry sample.

Based on the measurements of the thermal conductivity in the saturated pellets with different void ratios (Fig. 3), the saturated thermal conductivity is set to 1.3 W/mK taking the fact into consideration that the void ratio of the sample is equal to 0.797 (Fig. 3). In Tien et al. 2015, thermal conductivity of different Bentonite-based materials of different compositions were measured under different water content. These measurements indicate that the dry thermal conductivity of the bentonite material varies from 0.3 to 0.45 and material of lower dry density has a lower dry thermal conductivity. According to that, the dry thermal conductivity is assumed as 0.3 in the modelling. The adopted function has been compared with the measured thermal conductivity of different void ratios (Fig. 4, left) and different dry density (Fig. 4, right). Generally the relations adopted in OGS can represent the trend of thermal conductivity evolution with respect to the change of saturation degree relatively well. However, especially at low saturation, it tends to underestimate the measured thermal conductivity. Generally, material of larger void ratios and low dry density exhibit a generally lower thermal conductivity. Furthermore, the adopted function was also compared with the measurements of Tang and Cui, 2010, in which the relationship between the thermal conductivity of compacted MX80 and the water saturation was measured (Fig. 5). In this comparison the most experimental data relate to the adopted curve quite well.

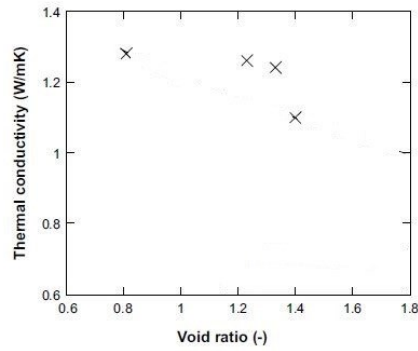


Fig. 3: Measured thermal conductivity of the saturated MX80 pellets with different void ratios (Börgesson et al. 1994)

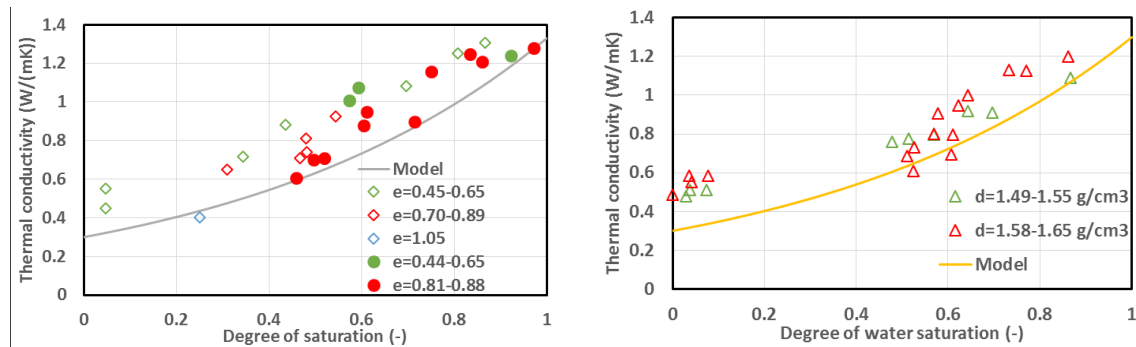


Fig. 4: Comparison of the adopted relations in the code OGS with the measured thermal conductivity of Bentonite (Left: given for different void ratio of MX80 (/Kahr and Müller-Vonmmos 1982/: \diamond ; /Börgesson et al. 1994/: \circ); right: given for different dry density of Febex (Villar 2002)

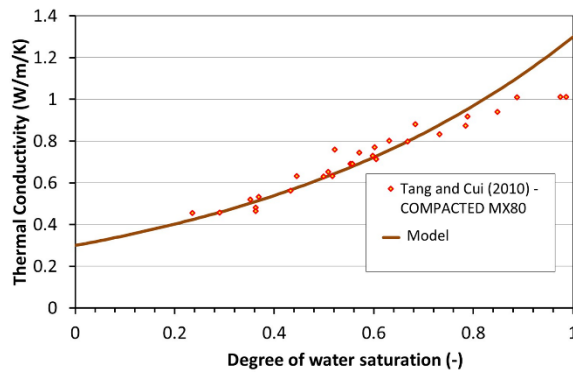


Fig. 5: Comparison of the adopted function with the measurements of compacted MX80 in Tang and Cui 2010

2.3.3 Modified van Genuchten function

A widely used type of retention curve for clayey materials is the van Genuchten function (Eq. (26)). In (Jacinto et al. 2009) the water retention behaviour of MX80 bentonite and sand-bentonite mixture under different temperature were measured. The measured results indicate that the capacity of water retention in both material reduces when the temperature increases (Fig. 6) that means at the same degree of water saturation, the corresponding suction at the high temperature is lower than that at the low temperature. To take into account the temperature effects on the water retention, the van

Genuchten function is modified with the assumption that the pore size index m_T and the maximal water saturation S_{mT} are temperature dependent, that can be given by:

$$\begin{aligned} m_T &= m_0 + \eta_m (T - T_0) \\ S_{mT} &= S_{m0} + \eta_s (T - T_0) \end{aligned} \quad (34)$$

where T_0 is the initial temperature m_0 and S_0 are the parameter of van Genuchten function at the initial temperature T_0 . With the modified van Genuchten function the tendency of the measured water retention behaviour of MX80 bentonite at different temperatures can be well described (Fig. 6).

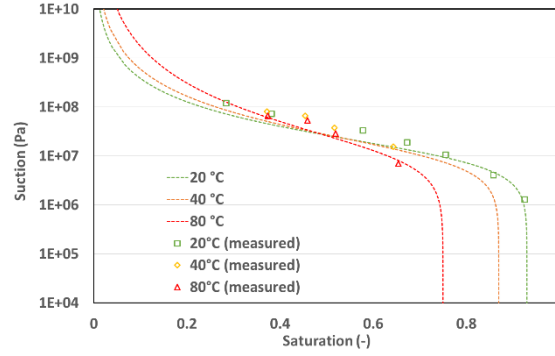


Fig. 6: Comparison of the measured water retention curves with the adopted modified van Genuchten function at different temperature

2.3.4 Swelling and shrinkage behaviour

Clayey material exhibits strong swelling/shrinkage behaviours when the water content changes. Due to the presence of bedding, clay rock have a strong anisotropic THM properties. According to the measurements in the laboratory heating experiments on COX [EP1] the additional strain increments in the mechanical process caused by swelling/shrinkage are assumed as anisotropic and dependent on the orientation to bedding. Generally the increase of water content (suction decrease) leads to swelling and in the contrary the decrease of water content (suction increase) causes shrinkage. The strain increments can be expressed as:

$$d\varepsilon_s = \frac{-dS}{d\mathbf{K}_s} \quad (35)$$

where $S = p^g - p^l$ is the suction, \mathbf{K}_s is the bulk modulus tensor against suction change. Considering the transversely isotropic swelling/shrinkage, different value of bulk modulus parallel to bedding K_s^{\parallel} and perpendicular to bedding K_s^{\perp} are defined.

For bentonite the swelling/shrinkage behaviour was considered by an additional stress in the mechanical field which has a simple, linear relationship with the change of water saturation:

$$\Delta\sigma_{sw} = -\sigma_{sm} \Delta S^l I \quad (36)$$

Where σ_{sm} is the maximum swelling pressure.

3 Model validation and interpretation

The developed numerical model has been applied to simulate a laboratory heating experiment on COX [EP1], laboratory long-term heating and hydration experiments on MX80 bentonite [EP2], and the in situ HE-E heating experiment [EP3].

3.1 Modelling of the laboratory heating experiment on COX

3.1.1 Experiment description

This laboratory heating experiment on the COX was carried out by GRS (Zhang et al., 2010) with main purpose to characterise the TH properties of the COX. The sample was mounted on a triaxial apparatus (Fig. 7, left). Heating was accomplished using an electrical heater positioned near the bottom of the sample. During heating the sample was loaded with an axial stress of 15.5 MPa and a confining stress of 15 MPa. The water back-pressure at the bottom and the top of the sample, the axial deformation and the radial deformation were monitored throughout the experiment. The experiment was constructed with several different phases (Fig. 7, right). In the modelling only the heating process was simulated. Before heating synthetic COX pore water was injected into the sample through the upper and lower porous discs for 67 days until that the sample was saturated. After that under undrained and adiabatic conditions heating phases was started. Firstly, temperature was increased from 30 °C to 60 °C with a rate of 3 °C/h. Then it remained constant at 60 °C for about 3 days. After that, the second step started with temperature elevation from 60 °C to 90 °C with a rate of 1.2 °C/h. Until the end of the test, the temperature was kept constant of 90 °C. In the modelling only the first two phases are considered (until to 76 days in Fig. 7, right). Heating has generated a strong pore pressure response at the bottom and the top of the sample. In the first heating step (from 30 °C to 60 °C) a rapid increase of the pore pressure from the initial value of 1.2 MPa to 4.3 MPa at the top and to 7 MPa at the bottom was measured. Afterwards the pressure decreased at the elevated constant temperature level gradually to 2.2 MPa at the top and to 1.7 MPa at the bottom. In the second heating step (from 60 °C to 90 °C) the pore pressure increased rapidly to 6.5 MPa at the top and to 11.7 MPa at the bottom. Similar to the first heating phase, the pore pressure decreased continuously when the temperature remained constant at 90 °C.

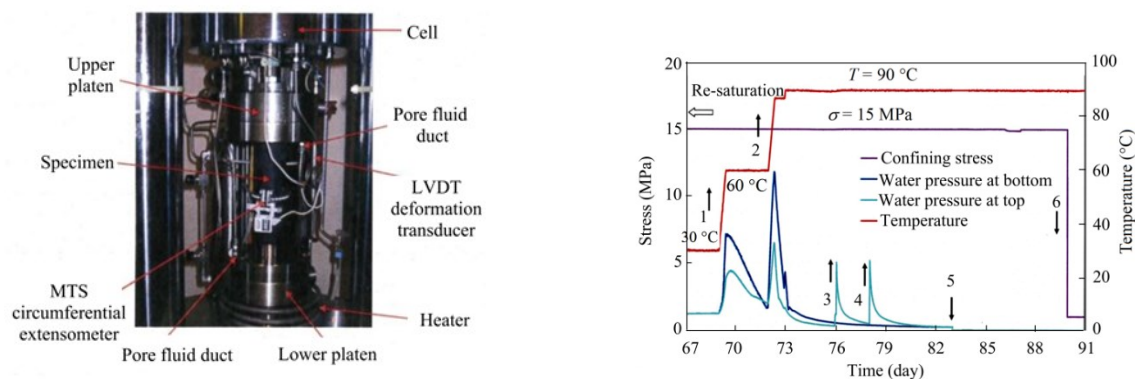


Fig. 7. Triaxial testing apparatus (left), the heater temperature, confining stress, and the measured pore pressure at the top and at the bottom of the sample (right) (Zhang et al., 2010).

3.1.2 Model set up

An axisymmetric model with a height of 100 mm in the direction of the rotational axis (y-direction) and a radial of 25 mm (x-direction) was constructed to simulate this heating experiment (Fig. 8). The bedding is in the direction perpendicular to the rotational axis and represents the transversely isotropy of the clay sample. According to the experimental observations that in both heating stage the elevated pore pressure dissipated at the constant high temperature even under the undrained conditions, thus a possible leakage was suggested (Zhang et al., 2010). This argument have also been proved by an analytical analysis based on the Tait equation and a numerical simulation without leakage effect [EP1]. Therefore, leakage points were assumed in the model (Fig. 8), at which the pore pressure was fixed at the atmospheric pressure. The coupled thermal, non-isothermal multiphase flow and mechanical model (TH²M) was applied to simulate this laboratory test. The most model parameters (Table 1) are derived from the experimental data base (Zhang et al., 2010). The THM transversely isotropy of the bedded clay formation were considered and represented by transversely isotropic values. The physical properties of water and dry air were assumed equal to the typical value under the standard state. Additionally temperature dependent thermal expansion and viscosity are implemented for water [EP1].

Table 1: Model parameters for COX

Parameter	Symbol	Unit	Value ()
Solid grain density	ρ_s	kg/m ³	2552
Young's modulus	E	GPa	10 / 4
Possion's ratio	ν	-	0.24/0.33
Biot constant	a	-	1
Porosity	ϕ	-	0.053
Permeability	K	m ²	$4.5 \times 10^{-20} / 5 \times 10^{-21}$
Permeability enhancement factor	β	-	Eq.((32))
Thermal expansion	α_s	K ⁻¹	0.9×10^{-5}
Specific heat capacity	C_s	J·Kg ⁻¹ ·K ⁻¹	800
Thermal conductivity	λ_s	W·m ⁻¹ ·K ⁻¹	2.2 / 1
Critical pore pressure	p_{cri}	Pa	7.2 (Eq. (32))
Swelling coefficient	$\gamma_s = 1/k_s$	GPa ⁻¹	1.6 / 1 (Eq.(35))

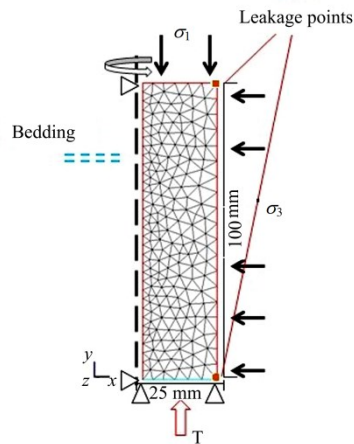


Fig. 8: Sketch of the numerical model: geometry, mesh and the boundary conditions.

3.1.3 Results analysis

Fig. 9, left shows the response of pore pressure to the temperature change at the top and bottom of the sample. The increase of pore pressure as the temperature rise is caused by the thermal expansion of each phase: solid, water and gas. With the leakage points the drop down of the pore pressure at the elevated constant temperature can be satisfactorily reproduced. If the permeability was assumed as constant an extremely high pore pressure in the second heating stage of high temperature (more than three times the measured pore pressure) was calculated (dashed line in Fig. 9, left). A good agreement between the measured and calculated pore pressure can be achieved by the modelling using the pore pressure dependent permeability. Compare to the behaviour in the first heating phase, the pressure dropped down more rapidly in the case of constant temperature in the second heating phase. Due to the high pore pressure, possible pore space expansion may happen. This additional expansion of pore space can also be simulated using the abovementioned pressure dependent permeability model. The simulated results indicate that the drop of pressure is not only due to the leakage but also due to the increase of permeability. The different strain evolution (Fig. 9, right) between the radial and axial direction were mainly caused by the anisotropic properties of the sample. To be specific, the sample has a smaller thermal conductivity, a weaker shrinkage/swelling behaviour and a smaller stiffness in the direction perpendicular to bedding (axial direction) than that in the direction parallel to bedding (radial direction). As the temperature increases, the increase of extension strain in radial direction was caused by the thermal expansion and by the pore pressure increase (Fig. 9, right). Only relatively small extensive strain ($< 0.05\%$) was measured and calculated because of the relative high confining stress of 15 MPa. The compressive behaviour of the sample at the constant temperature was mainly caused by the consolidation process following the leakage. And the more rapid compression behaviour of the sample during the second heating phase than during the first heating phase may indicate a plastic material behaviour which has caused an irreversible permeability enhancement. To analysis the gas effects, the first heating phase was additionally simulated using a coupled non-isothermal Richards flow mechanical model, in which the gas mobility and change of gas pressure are neglected. The calculated pore pressure evolution have been compared with the measured one (Fig. 10). It is verified that the present of gas in porous medium can affect the pore pressure evolution significantly. The effects could be from two aspects: 1) the phase change from liquid phase to gas phase can equilibrate the change of liquid field; 2) the gas expansion could have impact on the pore pressure evolution [EP1].

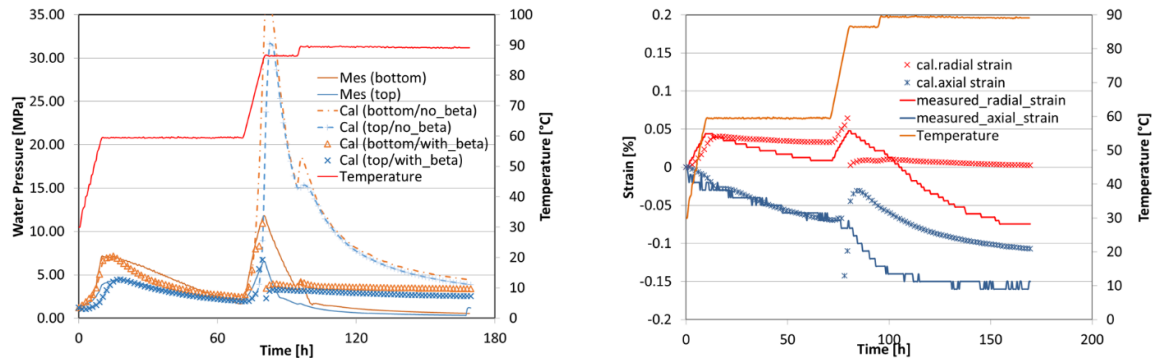


Fig. 9: Comparison of the calculated results of COX with the measured data (left: pore pressure evolution; right: axial and radial strain).

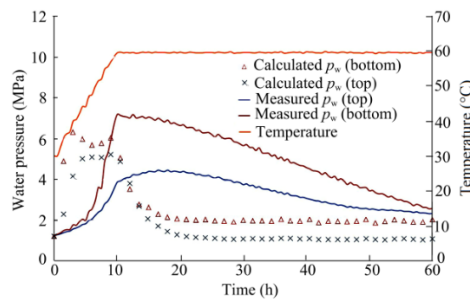


Fig. 10: Comparison of the computed pore pressure by using the Richards flow model (single phase) with the measured data.

3.2 Modelling of the laboratory column test on the granular MX80 bentonite

3.2.1 Experiment description

Since 2012 CIEMAT is performing a long-term laboratory heating and hydration test on the MX80 (sodium bentonite MX80 from Wyoming, USA) pellets (Villar, 2012; Villar et al., 2014). This experiment is conducted as complementing to the HE-E in situ heating experiment (Teodori and Gaus, 2011). The purpose of this experiment is to estimate the buffer material properties under the conditions of fewer uncertainties. By the test the MX80 column is installed inside the cell. The heater is installed in a steel frame that has direct contact to the bottom of the sample (Fig. 11, left). To reduce heat losses and for a better heat transfer heater, the cell wall and the outside of cell were replaced with different insulation materials. At 1518 h, the insulation system was improved by replacing the 5mm dense foam with a 30 mm insulation wool. The detail of the insulation system can be found in (Villar, 2012). Three sensors (sensor 1 at 40 cm from the sample bottom, sensor 2 at 22 cm, and sensor 3 at 10 cm, respectively) are placed in the cell to record the temperature and humidity evolution. The axial pressure on the top of the sample and the water intake are also monitored during the experiment. The experiment was conducted with two heating phases followed by a hydration phase (Fig. 11, right). The first heating phase lasted from the beginning to 3524 h. The maximum temperature at the heater during the first heating phase was kept as constant at 100 °C. After that, the second heating phase was started (from 3524 to 5015 h) in which the heat power was increased and the final temperature at the heater was kept at 140 °C. After 5015 h of heating, the hydration phase was started with water injection from the opposite of the heater with a constant water pressure of 0.1 bar. During hydration, the temperature at the heater is maintained at 140 °C.

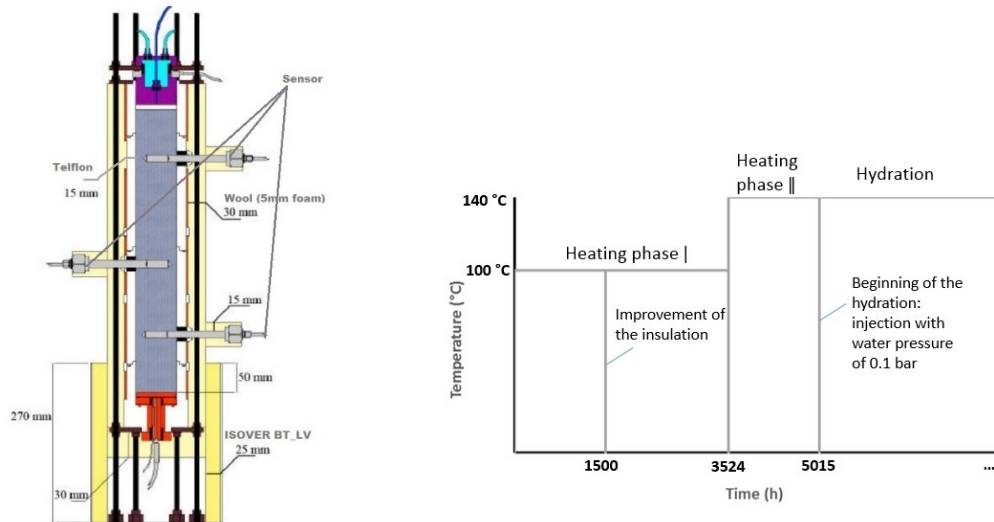


Fig. 11: Sensors and Insulation systems around the MX80 sample (Villar, 2012) (left), phases of the experiment (right)

3.2.2 Model set up

This experiment was simulated using a coupled non-isothermal multiphase flow mechanical model. According to the experimental layout (Fig. 11, left), an axisymmetric model (Fig. 12, left and middle) was generated under the assumption of the symmetric experimental conditions. The model was divided into seven material groups for the different experimental components: the bentonite column, heater element, low part of the heater, steel support line and several thermal insulations [EP2]. In the model, the groups standing for insulation wool and ISOVER BT-LV were initially assigned with dry air parameters from the beginning to 1500 hours (Fig. 12, left). After 1500 hours, due to the improvement of the insulation, they were defined as two different insulation materials with corresponding material parameters (Fig. 12, middle). The room temperature of 21.5 °C was assumed as the initial temperature of the model domain. The initial saturation degree is set to 22% for the bentonite group corresponding to the measurements. The initial gas pressure was assumed as the atmospheric pressure of 1 bar. The upper and lateral boundaries were assigned with the measured laboratory temperature (Fig. 12, right). The heat source term was added along a polyline inside the material group 'Heater' that is corresponding to the real heat power. An empirical heat loss coefficient of 0.25 was applied by the heat source term in consideration of the fact that heat flux can escape from the space between the different experimental components and flow into the lower part of the heater. The hydration phase was simulated by applying an additional constant water pressure of 0.1 bar at the top of bentonite. According to the experimental conditions, the movement of the bentonite boundaries was restricted.

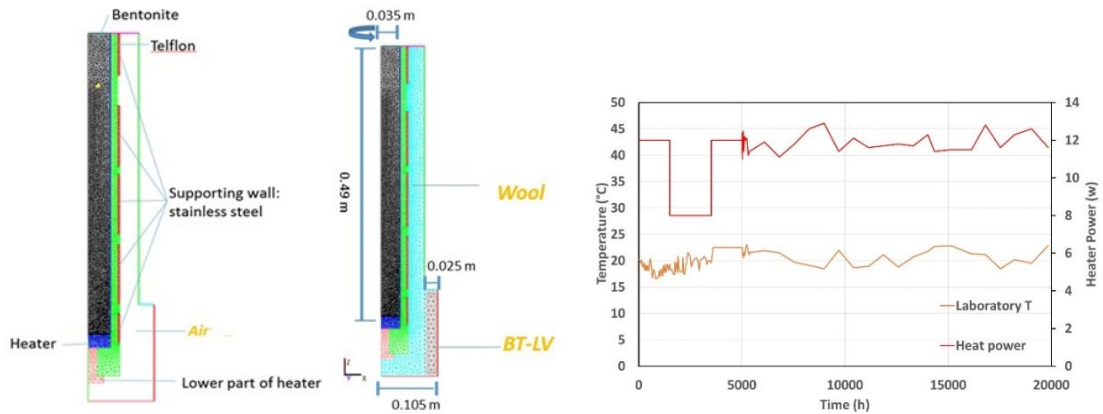


Fig. 12: Model geometry and mesh (left: before 1500 h, middle: after 1500 h); measured laboratory temperature and heat power (right)

The relevant model parameters for the MX80 bentonite are listed in Table 2. The most parameters are based on the laboratory measurements in (Villar, 2012). The determination of the intrinsic permeability is based on the back-analysis of the measured water intake during the hydration phase. Saturation dependent thermal conductivity was applied in the modelling (section 2.3.2). Modified van Genuchten function (section 2.3.3) was applied to describe the water retention behaviour of the MX80. The in table listed is the van Genuchten parameters at the reference temperature of 25 °C that were determined by fitting the corresponding measured retention curve. The swelling/shrinkage behaviour was described by (Eq. (36)).

Table 2: Parameters of the MX80 bentonite

Material	Property	Value	Unit
Bentonite	Dry density	1530	kg/m ³
	Young's modulus	18	MPa
	Poisson ratio	0.35	-
	Porosity	0.44	-
	Intrinsic permeability	4.5×10^{-21}	m ²
	Liquid relative permeability	$k_{rel}^l = (S^l)^5$	-
	Gas relative permeability	$k_{rel}^g = (1 - S^l)^5$	-
	Air entry pressure	28.6	MPa
	Water retention m	0.512	-
	Saturated thermal conductivity	1.3	W/(m·K)
	Dry thermal conductivity	0.3	W/(m·K)
	Specific heat	950	J/(kg·K)
	Maximum swelling pressure	8 (Eq. (36))	MPa

3.2.3 Results analysis

3.2.3.1 Results of heating phase

Fig. 13 depicts the results comparison during the heating phases. Due to the low thermal conductivity a significant temperature gradient is generated within the sample (Fig. 13, left). The increase of temperature at 1500 hours under the constant heater temperature was caused by the improvement

of the insulation system the can be well reproduced in the model through modification of the corresponding material parameters (Fig. 12, left, middle). In general, using the saturation dependent thermal conductivity the calculated temperature especially in the middle and upper part of the bentonite sample (sensor 1 and 2) matches the measured data quite well. However, the temperature in the lower part (sensor 3) is slightly overestimated. Several factors may cause the difference between the calculated and measured results [EP2]. One factor could be the generation of local micro fissures due to the shrinkage deformation caused by heating, which could change the mechanism of heat transfer and accelerate the heat advection upwards. Another factor could be the underestimation of thermal conductivity at lower water saturation due to insufficient experimental data. Additionally, a reference modelling using constant thermal conductivity of 0.5 for MX80 was carried out. The results (dashed line in Fig. 13, left) show a general overestimation of temperature at the sensors however underestimation of the temperature at heater. At the beginning of heating the increase of temperature caused water evaporation in area close to the heater and drove water upwards. Thus, the humidity at the sensors increased (Fig. 13, right). Afterwards, the sensor 3 was under high temperature, and humidity decreased continuously until to the time of 3524 hours. At the beginning of the second heating phase, the temperature jump from 100 °C to 140 °C caused additional vaporisation and vapour in-flux from the bottom of the sample, which led to the increase of humidity at sensor 2 and sensor 3. At sensor 1, a relatively smooth increase in humidity was obtained both in the numerical results and in the experiment measurements. A good agreement is reached between the measured and calculated results since the temperature effects on water retention behaviour is taken into account. In contrary, neglecting the temperature effects leads to a general underestimation of the relative humidity especially under the high temperature (dashed line in Fig. 13, right). Still the temperature at sensor 3 is underestimated during the second heating phase. One reason could be the overestimation of the temperature evolution at sensor 3 during this time (Fig. 13, right). Another reason could be related to the possible generation of micro-fissure in this area under such high temperature.

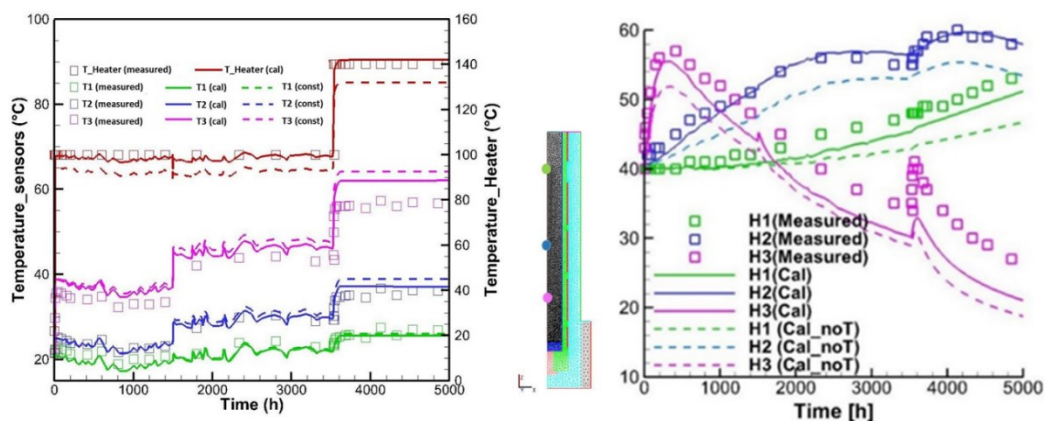


Fig. 13: Results of the heating phase (left: temperature, right: relative humidity)

3.2.3.2 Results of hydration phase

During the hydration phase temperature within the sample was kept approximately constant. Only an oscillation of about ± 2 °C can be observed at each sensor (Fig. 14, left). These oscillations are mainly due to the thermal conductivity caused by water saturation redistribution. As water is taken into the

sample from top to bottom, the humidity at sensor 1, which was located near the top of the sample, increased progressively at the beginning of the hydration (Fig. 14, right). At sensor 2 and sensor 3 the decrease of humidity was observed and calculated at the beginning of hydration which is due to the continuous water evaporation and the vapour flux upwards. Afterwards humidity increased steadily as the injected water reached this lower area. The response of humidity at sensor 3 is relatively slight due to the large distance to the top. Generally the process of humidity recovery is underestimated in the modelling. One possible reason could be the assumption of the homogenous and constant permeability for the whole model domain. Permeability may be increased due to the potential appearance of micro-fissures in the lower part of sample.

The calculated water intake and axial pressure together with the measured data are illustrated in Fig. 15. The calculated water intake matches the measurements quite well for the first 2000 hours. However, after 2000 hours the rate of the calculated water intake is significantly lower than the measured one. The rate of water intake is mainly controlled by the hydraulic permeability and gradient of pore pressure. The measured large amount of water intake after 2000 hours may indicate the extensive additional void space which is correlated to an increase in permeability. One of the possible reasons may be the generation of micro-fissures caused by shrinkage in the lower part which is under high temperature. A stationary state is not reached even after 15000 hours. Theoretically, the sample can take in about 800 g water in total. Under the constrained laboratory conditions, the increase of axial pressure is mainly generated by the swelling behaviour of the sample. From the measured data, it can be seen that the pressure already reached 1.4 MPa after about 3000 hours (Fig. 15) and kept approximately constant until 15000 hours. However, the calculated axial pressure increased progressively until 15000 hours. The sample was numerically assumed as a homogeneous continuum, using the current swelling stress formulation (Eq. (36)). Water can successively flow into it and swelling pressure can progressively build up. However, if micro-fissures have been generated by shrinkage in the lower part of the sample during the heating phase, they may be sealed due to the swelling behaviour of bentonite during hydration. Swelling pressure will be released through the sealing process. That could be a reason for the observed axial pressure remaining approximately constant in late hydration phase. The total measured axial pressure may increase again as long as all the micro-fissures are sealed through the swelling deformation. This interaction can only be proven by a long-term experimental observation.

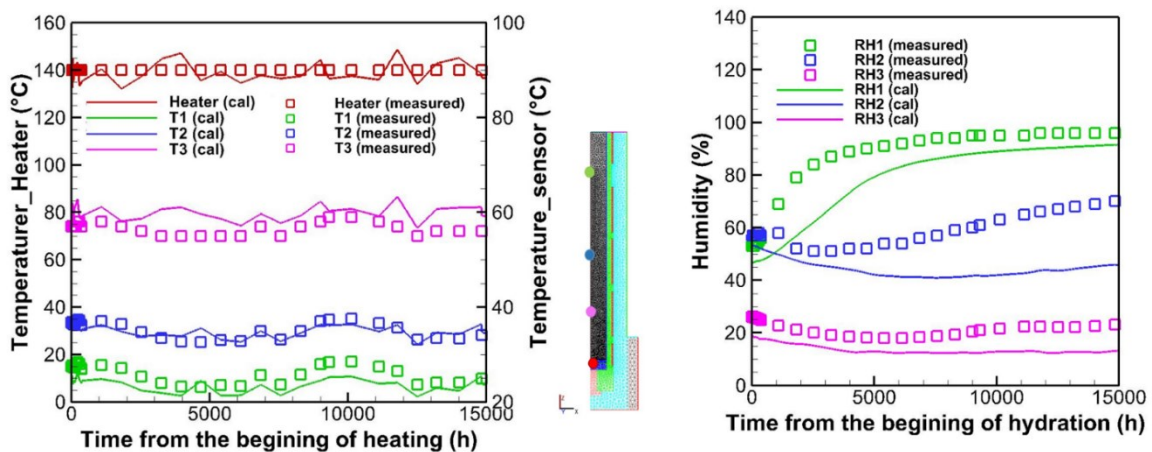


Fig. 14: Results of the hydration phase (left: temperature, right: relative humidity)

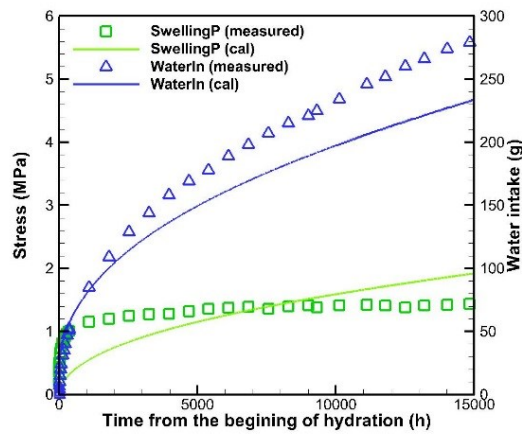


Fig. 15: Comparison of the calculated axial pressure and water intake with the measured data

3.3 Modelling of the HE-E in situ heating experiment

3.3.1 Experiment description

The HE-E in situ experiment is a 1:2 scale heating experiment aimed at improving the understanding of the thermal evolution and the thermally induced HM interactions in the bentonite EBS and in the near field of the Opalinus Clay host rock, as well as providing experimental data for the calibration and validation of the numerical models (Teodori and Gaus, 2011). The HE-E test is performed in a 10-m long section of a 50-m long microtunnel of a 1.3 m diameter which was excavated in 1999 in the Opalinus Clay of the Mont Terri URL in Switzerland (Fig. 16, left). The HE-E experiment consists of two independently heated sections of 4 m length each. At each section heaters are placed in a steel liner supported by MX80 bentonite blocks. In each section, a heater is placed in a steel liner supported by MX80 bentonite blocks. The remaining space is filled with granular buffer material: the first section (referred to as section S/B) is filled with a 65/35 granular sand-bentonite mixture and the second section (B) is filled with pure MX80 bentonite pellets (Fig. 16, right). The thermal-hydro properties of both buffer materials have been characterised in the laboratory by means of performance of long-term heating and hydration column test (Villar, 2012). The heating started in June 2011. The target maximum temperature of 140 °C at the heater surface was reached in June 2012 after 1 year of heating. Since then the temperature at the heater surface are kept as constant at 140 °C.

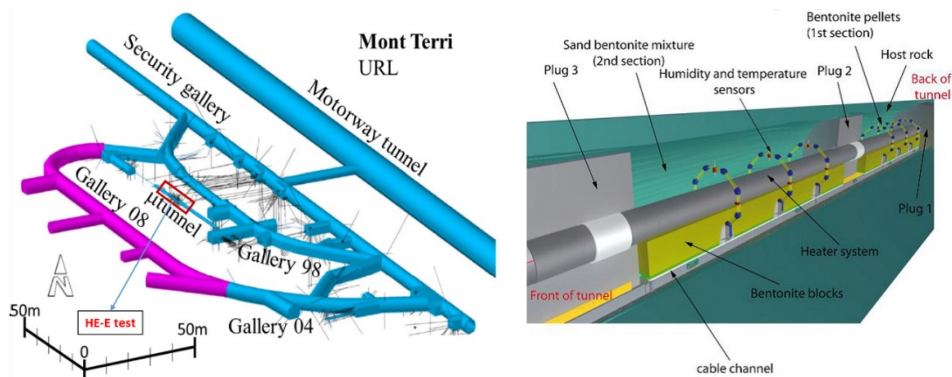


Fig. 16: Location (left) and schematic layout of HE-E experiment (right) (Teodori and Gaus, 2011)

3.3.2 Model features

A three-dimensional coupled THM analysis was performed (Fig. 17). The computation domain is centred on the length axis of the microtunnel. The HE-E test section is located at a distance between 27.5 m and 37.5 m away from the model front. All the relevant experimental components were considered in the model, with the definition of different material groups for 'intact rock', the 30 cm thick 'excavation damage zone (EDZ)', the cylindrical 'heater elements' with a diameter of 30 cm, 'bentonite blocks', 'three plugs', 'MX80' and the 'sand-bentonite mixture' buffer materials. The bedding was assumed to be rotated 40° anti-clockwise from the y-axis. Initial temperature was assumed as constant as 15 °C. The initial pore pressure was set to 0.9 MPa corresponding to the field-measured value. According to these measured results (Wermeille and Bossart 1999, Martin and Lanyon, 2003), major, intermediate and minor principal stresses of 7 MPa, 5 MPa and 3 MPa were assigned in vertical direction and in horizontal direction parallel and perpendicular to the tunnel axis respectively. Totally five modelling stages were considered: 1) Tunnel excavation, 2) 12-year ventilation after the tunnel excavation, 3) Emplacement of the granule buffer material and the bentonite block 4) 2898 days of heating 5) 50 years after shut-down of heater.

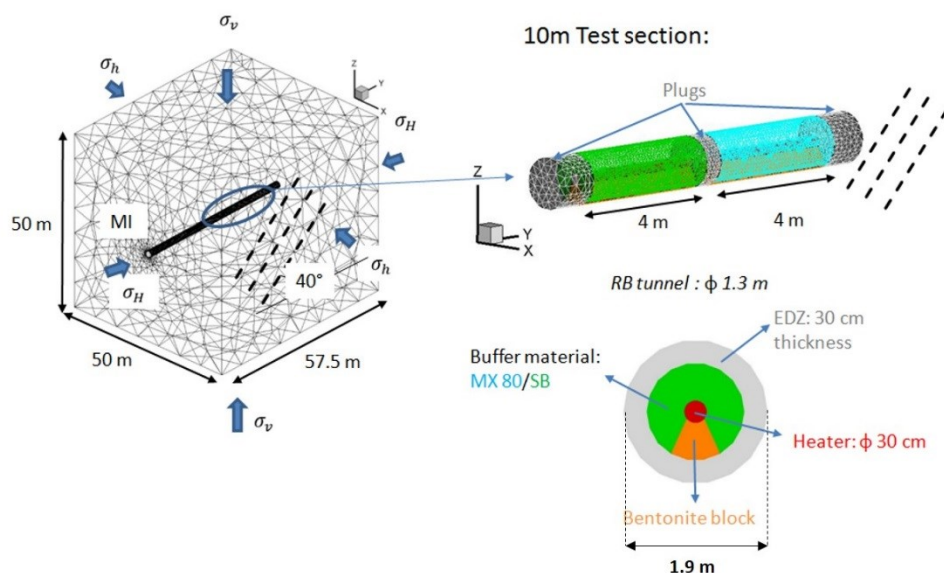


Fig. 17: Finite element mesh and model domain with geometry, material groups, and the initial stress

The coupled non-isothermal Richards flow and mechanical model was applied to simulate the HE-E test. The relevant model parameters are listed in Table 3. The parameters of the Opalinus Clay is based on the studies by (Wileveau, 2005). The parameters of the buffer material are derived from the experimental database (Villar, 2012) and the associate numerical analysis [EP2]. For the Opalinus Clay, some parameters (Young's modulus, Poisson's ratio, permeability, thermal conductivity) have different values depending on the orientation of the material either parallel or perpendicular to the bedding. This reflects the anisotropic mechanical, hydraulic and thermal properties of the clay formation caused by the bedding. It is assumed that the EDZ has higher hydraulic conductivity than intact clay: the porosity is greater and the permeability is five times the permeability of the host rock. The saturation dependent thermal conductivity (section 2.3.2) is adopted for the MX80 pellets, the sand-bentonite mixture the bentonite block. The dry and saturated thermal conductivities are given

in the table. The value of the dry and saturated thermal conductivity of the MX80 bentonite is taken from the modelling of the column test [EP2]. And the value of the sand-bentonite mixture and the bentonite block were determined through fitting the measurements from (Wieczorek et al., 2011). The Van Genuchten function were adopted to describe the water retention behaviour of each material. The corresponding van Genuchten parameters were determined based on the corresponding experimental data base (measurements on Opalinus in (Ferrari and Laloui, 2012) and (Romero and Gomez, 2013), measurements on the MX80 bentonite in (Rizzi et al., 2010) and measurements on the sand-bentonite mixture and on the bentonite block in (Wieczorek, 2013).

Table 3: Model parameters of HE-E modelling

	Symbol	Clay (EDZ (MX80 (Sat/Unsat)	SB (Sat/Unsat)	Block (Sat/Un sat)	
Dry Density (kg/m ³)	ρ_{dry}	2450	2450	1627	1383	1806	
Young's modulus (MPa)	E	9300/5800	9300/5800	18	18	24	
Poisson ratio (-)	ν	0.33/0.4	0.33/0.4	0.35	0.35	0.2	
Biot coefficient (-)	α	0.6	0.6	1	1	1	
Bishop coefficient (-)	χ	1.4	1.4	1.4	1.4	1.4	
Specific heat (J/(kg.K))	c	995	995	950	800	800	
Porosity (-)	ϕ	0.137	0.15	0.46	0.467	0.4	
Thermal conductivity (W/(m.K))	λ	2.15/1.2	2.15/1.2	1.2/0.35	1.3/0.3	1.3/0.8	
Thermal expansion (K ⁻¹)	a_n	1.4×10^{-5}	1.4×10^{-5}	2.5×10^{-5}	2.5×10^{-5}	2.5×10^{-5}	
Permeability (m ²)	k_{int}	$1 \times 10^{-19} /$ 1×10^{-20}	$5 \times 10^{-19} /$ 5×10^{-20}	3.5×10^{-20}	1×10^{-19}	2.5×10^{-21}	
Water retention*	Air entry pressure (MPa)	p_0	18	2	11.5	1.67	30
	Shape factor (-)	m	0.4011	0.4011	0.388	0.35	0.4
	Maximal/residual Saturation	$S_{max} /$ S_{res}	0/1	0/1	0/0.93	0/1	0/1
Initial Saturation	S_{int}	1	1	0.2	0.11	0.63	

3.3.3 Results analysis

3.3.3.1 Results of the ventilation process

The excavation and ventilation processes created a strong hydraulic gradient (Fig. 18, left) and an unsaturated area (Fig. 18, right). The unsaturated state around the tunnel could result in a relative slightly thermally induced pore pressure increase in this area during the heating phase even under a relative relative high temperature.

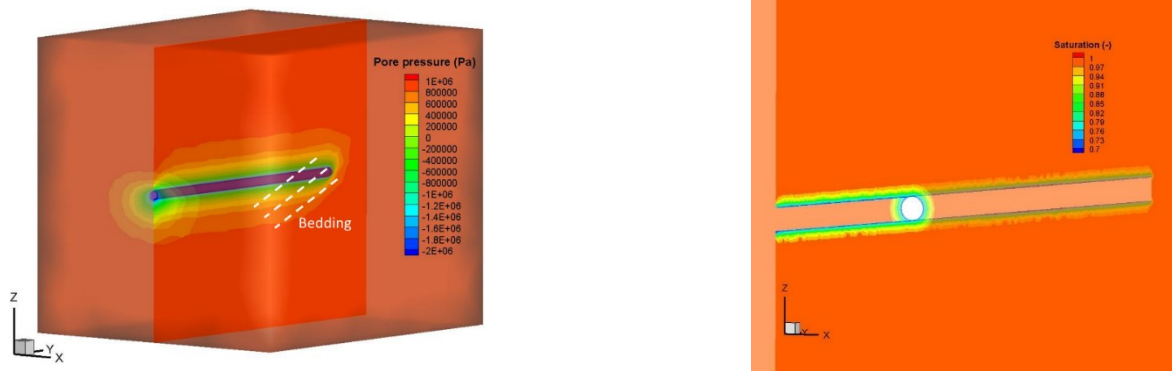


Fig. 18: Calculated distribution of pore pressure (left) and water saturation (right) after 12 years of ventilation

3.3.3.2 Results of the heating phase

EBS behaviour

(Fig. 19) illustrates the comparison of the computed temperature with the measured one. The measured suddenly drop-down of temperature indicates the disruption of heating that caused by a few electricity supply indents. Such interruption of heating was not considered in the modelling. By applying the actual heating power as a thermal source term at the heater surface, the observed temperature evolution at the heater surface can be easily reproduced in both heating sections. The temperature at the heater surface was not entirely homogeneously distributed. The temperature in the upper part was slightly higher than the temperature in the lower part, owing to the higher thermal conductivity of the bentonite block compared to the pellet material. An additional factor which caused this inhomogeneous temperature distribution could be the upward move of the dry air.

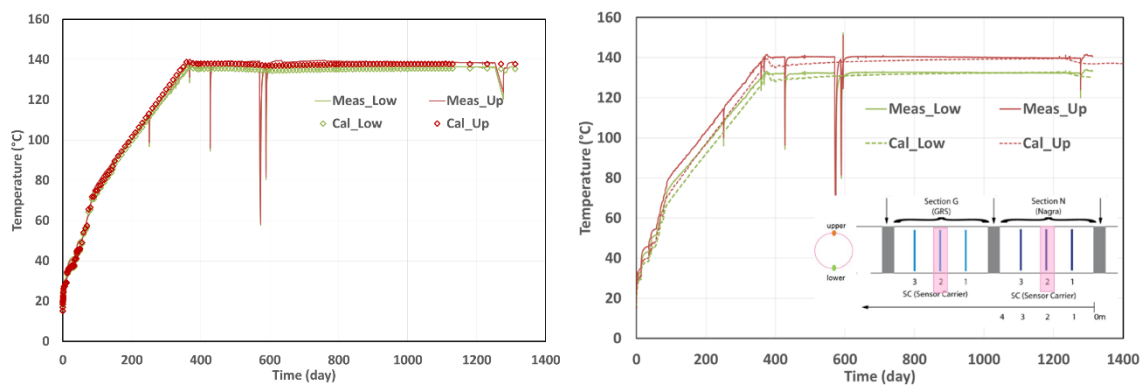


Fig. 19: Comparison of the calculated temperature evolution at lower and upper heater surface with the measured data (left: in B section, right: in S/B section)

The most important behaviours of EBS are the temperature and humidity evolution. Particularly, critical parameters here for the evolution of temperature and humidity are the thermal conductivity and the water retention function. Fig. 20 illustrates the results comparison of temperature and humidity at three sensor points in the middle measurement plane of the section B (MX80 bentonite). The most experimental observations can be satisfactorily reproduced in the modelling: e. g. the strong temperature gradient (from 140 °C to 40 °C) in the buffer material due to the low thermal conductivity, the relative low temperature of 45 °C at the interface (12H) between the EBS and host rock. In the later heating phase ($t > 1000$ hours) slightly decrease of temperature was calculated at all sensors as

the results of the recovery of water saturation slowly at those points following the water intake from the host rock to the EBS. The emplacement of buffer material and bentonite blocks induced a strong increase in humidity at the interface because the water was pulled out from the Opalinus Clay by the strong suction in the buffer material. This increase of humidity at the interface can be well represented by additional simulation of the 90-day emplacement stage. There is no significant change in humidity at other points with a certain distance to the host rock (Fig. 20, right). At the beginning of the heating period, a slight increase in humidity was observed at all sensors, which was attributed to the inflow of the water vapour the zone between the sensors and the heater surface where the water was firstly evaporated under the high temperature. After that as the temperature increased, a desaturation process took place in the EBS near the heater. The continuous decrease in humidity near the heater is due to water evaporation and the subsequent vapour diffusion towards the cooler zone. The temperature at point 12M in section B was generally underestimated, while the temperatures at other points (heater, 12C and 12H) were well fitted. As a result, the humidity at point 12M was overestimated. The reason for such inconsistency could be a change in the thermo-hydro properties of the buffer caused by e. g: the formation of local micro fissures. However, there is no experimental evidence for such material failure. Additionally the neglecting of gas mobility, condensation process and the process of dissolution of gas into liquid phase could be further possible reasons. In the sand-bentonite and in the bentonite block, similar behaviours as in the MX80 bentonite were observed and calculated [EP3].

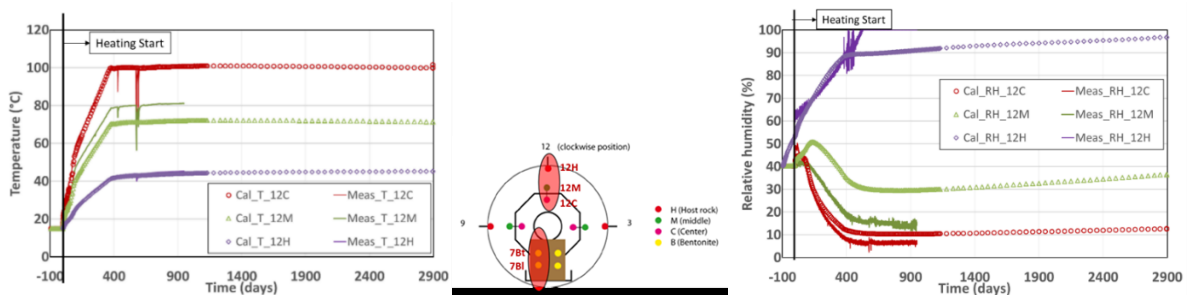


Fig. 20: Measured and calculated evolution of temperature (left), relative humidity (right) in MX80

Behaviour in the Opalinus Clay host rock

Temperature distribution and pore pressure evolution are two important issues in the clay host rock close to the heater. To compare the results, several points were selected in section SB2, that have a maximum distance of 1.5m (T-B16) and a minimum distance of 0.5 m (T-B10) to the heater surface. The calculated temperature evolution has a good agreement with the measured development, especially in the area close to the tunnel wall. In the far field, the temperature was slightly overestimated, which could result from the local heterogeneity (Fig. 21, left).

One area of increased pore pressure in the Opalinus Clay was calculated to be located at several metres from the tunnel wall and running parallel to the bedding (Fig. 21, right). This increase is due to the thermal expansion of fluid, solid and gas. Due to the relative low temperature (maximum temperature of 45 °C) in the Opalinus Clay, no extremely overpressure (e.g. higher than the minimum principal stress) was observed or calculated. The calculated pore pressure evolution in borehole BVE-1 was compared with the measured data (Fig. 22, left). This borehole was drilled from Gallery 98 (Fig. 16, left) and equipped with quadruple packers at 2 m intervals. Due to the simulation of the ventilation

process, the low initial pore pressure can be reproduced. The overall trend of the pore pressure evolution during heating can be captured in the model: the pore pressure increase during the first 400 heating days caused by the thermal expansion, and the later dissipation of the overpressure gradually following the consolidation process. However, the calculated pore pressure response was more intense than the observed behaviour. One possible reason for this difference in behaviour could be the underestimation of the storage capacity of the porous medium or the overestimation of the hydraulic conductivity in this area. Furthermore, the presence of Gallery 98 has certain effects on the pore pressure evolution in its vicinity, for instance where, packers P-B1-07 and P-B1-09 are located. To confirm these statements, a variation calculation was carried out. In this calculation, the permeability of Opalinus clay was reduced from $10^{-19}/10^{-20} \text{ m}^2$ to $5 \times 10^{-20}/5 \times 10^{-21} \text{ m}^2$ and the storage coefficient was increased from $1 \times 10^{-9} \text{ m}^{-1}$ to $2 \times 10^{-9} \text{ m}^{-1}$. The effects from Gallery 98 were considered by reducing the pore pressure at the left surface of the model 98 from 0.9 MPa to 0.1 MPa where is near to the Gallery. A better agreement between the measured and calculated pore pressure was reached in the variation calculation (Fig. 22, right). The results of the variation calculation indicates that except the permeability, storage capacity of porous medium is also a critical hydraulic parameter which is relevant to the poroelastic properties of the clay rock [EP3]. In addition to neglecting the gas flow, the gas thermal expansion could also be a further possible reason for the inconsistency between the measured and calculated pore pressure evolution (Fig. 21, Fig. 22). It was indicated in [EP1] that the gas phase in the pore volume acts as a buffer for the evolution of the pore pressure.

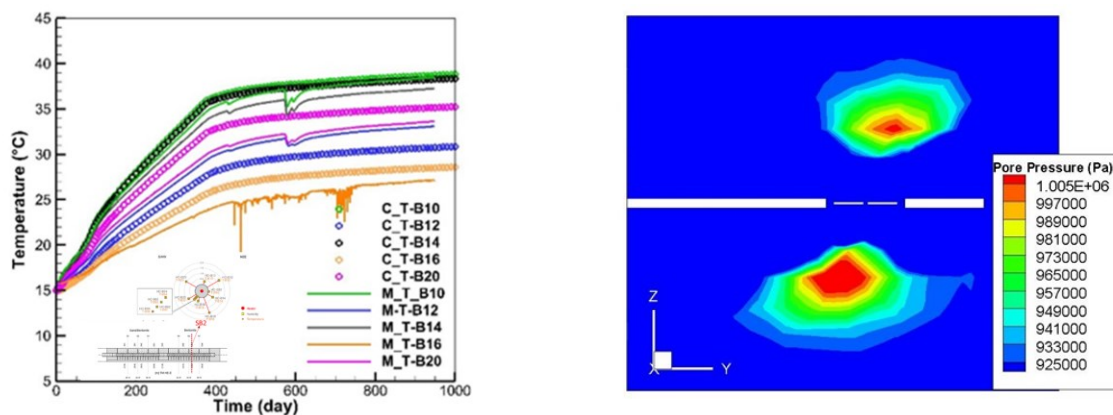


Fig. 21: Comparison of calculated temperature evolution with the measured one in the measurement section SB1 (left) and the calculated overpressure after 1500 days of heating

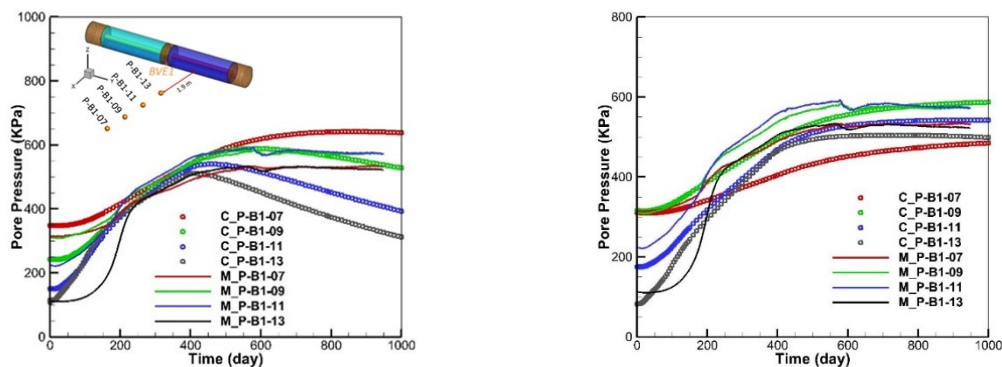


Fig. 22: Comparison of the calculated pore pressure (dots) evolution in Borehole BVE1 with the measured one (line), (left: basis calculation, right: calculation with low permeability, high storage capacity and the consideration of Gallery 98).

3.3.3.4 The long-term prognosis

In the long-term modelling the maximum extension of unsaturated zone, zone of elevated temperature ($>15\text{ }^{\circ}\text{C}$) and the resaturation process (Fig. 23, left) in EBS were predicted [EP3]. Additionally, variation calculations were performed, applying different levels of saturated water permeability of both buffer materials, to investigate the relationship between permeability and the time needed to reach the fully saturated state (Fig. 23, right). Two different behaviours (indicated in Figure with number 1 and 2) were recognised with respect to the increase of saturation time as a function of the decrease of saturated water permeability by both buffer material. When the saturated water permeability of MX80 is lower than $5 \times 10^{-21}\text{ m}^2$ and the permeability of sand-bentonite is lower than $2 \times 10^{-20}\text{ m}^2$ (area 1), the increase in saturation time is very steep, as is the decrease in permeability. And the gradients of time increase for the two buffer materials were different. Conversely, at high permeability (area 2), the saturation time increases slowly with the decreasing permeability. Considering the permeability of the Opalinus Clay as being between $1 \times 10^{-19}/1 \times 10^{-20}\text{ m}^2$, it may be concluded that, in case of a higher saturated water permeability of the buffer materials (e.g. MX80 higher than $5 \times 10^{-21}\text{ m}^2$, or sand-bentonite higher than $5 \times 10^{-20}\text{ m}^2$), the rate of water intake from the surrounding rock into the buffer will be mainly determined by the permeability of the Opalinus Clay.

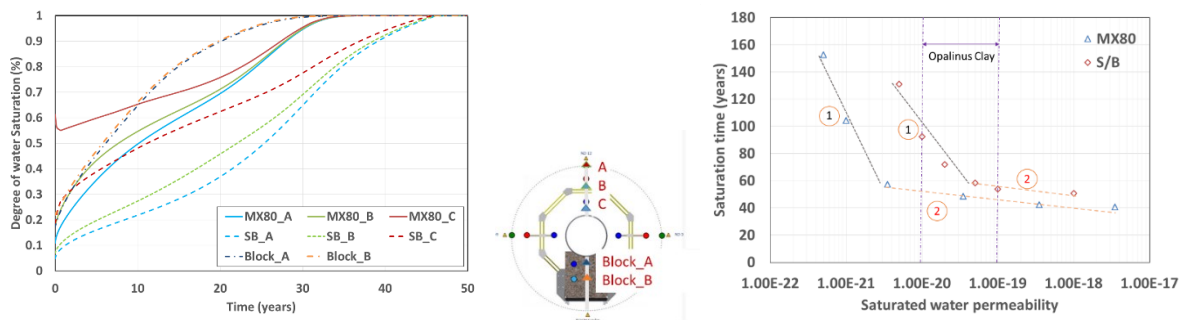


Fig. 23: Calculated saturation evolution after heat shut-down in the EBS (left), relationship between the saturated water permeability of buffer material and the saturated time

4. Conclusions and outlook

In this work, a coupled non-isothermal Richards flow mechanical model (THM) and a coupled non-isothermal multiphase flow mechanical (TH²M) model were developed to widen the understanding of the thermally induced THM interactions in the clayey material with respect to the repository of HLW. Special attention has been paid to the investigation of the coupling effects among the relevant material properties. The variation of the permeability due to the change of pore pressure, the relationship between the thermal conductivity and the degree of water saturation, the temperature effects on the water retention behaviour, and the swelling/shrinkage behaviour have been intensively analysed. Thereby the pore-pressure-dependent permeability model, the water-saturation-dependent thermal conductivity, the modified van Genuchten function considering the temperature effects, and the anisotropic swelling/shrinkage model for bedded clay formation were developed. The developed numerical model has been applied to simulate the experiments on clay-based material at different scales: the laboratory heating experiment on COX [EP1], the long-term heating and hydration

experiment on MX80 bentonite [EP2], and the HE-E in situ heating experiment [EP3]. Using the recent model concept, most of the experimental observations can be reproduced and interpreted well.

When saturated clay rock is subject to heating, a strong pore pressure response will be induced. The thermal expansion of solid and pore fluids will lead to an increase in the pore pressure. Afterwards, the elevated pore pressure will dissipate following the consolidation process. In the laboratory heating experiment on COX, if the permeability is assumed to be constant, a much more intensive pore pressure rise can be expected in the second heating stage due to the relatively high temperature. Considering the fact that the pore space structure could be changed by high pore pressure and as a consequence the permeability would be changed, the pore-pressure-dependent permeability model was developed. This permeability model has been applied to simulate the laboratory heating experiment on COX. It has been verified that the measured pore pressure evolution, especially at high temperature, can be fitted well only when the high-pore-pressure-induced permeability change is considered. Due to the presence of bedding, an obviously different behaviour of strain was measured between the radial and axial directions. By adopting the bedding-orientation-dependent swelling/shrinkage model, this different strain behaviour in the radial and axial directions can be interpreted. It was also indicated in the modelling of the heating experiment on COX that the gas has a so-called “buffer” effect on pore pressure evolution. De- and resaturation are two important processes during the closure phase of one disposal of HLW. Especially in the EBS, the temperature evolution could cause a significant change in the degree of water saturation. It has been estimated by many experiments and previous researches that the thermal conductivity of bentonite material is strongly dependent on the degree of water saturation. Based on the experimental measurements, a saturation-dependent thermal conductivity model was developed for bentonite. This thermal conductivity model was adopted in the simulations of the column test on MX80 pellets and the HE-E in situ heating experiment, which leads to a good agreement between the calculated and observed temperature evolutions. The high temperature could change the surface tension between the solid and fluid water and change the pore space structure, and therefore the water retention behaviour could be changed. Some experimental measurements of water retention curves indicated that the capacity of water retention at high temperature is lower than that at low temperature. Thus the classic van Genuchten function was modified to take into account the temperature effects on the water retention behaviour. In the simulation of the column test, the humidity evolution, especially at high temperature, can be better fitted only by adoption of the modified van Genuchten function. Additionally, in the modelling of the HE-E test, it was estimated through the variation calculations that the permeability of the EBS could have strong effects on the desaturation process, and the storage capacity of the clay rock was found to be one of the critical parameters for the thermally induced pore pressure response.

In future work, the numerical model can be improved with consideration of several aspects. For example, the distribution of the EDZ and the associated change in material properties, such as changes in permeability and mechanical strength, need to be considered. An elasto-plastic mechanical model complemented by a swelling/shrinkage model should be developed to take into account the possible formation of micro-fissures at high temperature and the sealing of the micro-fissures during the resaturation phase. The non-isothermal multiphase flow model should be completed with consideration of the condensation process and the process of gas absorption in pore water.

Reference

- Andersson C, Bàcena I, Bono N, Boergesson L, Cleall P, Forsmark T, Gunnarsson D, Johannesson L E, Ledesma A, Liedtke L, Luukkonen A, Pederson K, Puigomenech I, Pusch R, Rhén I, Rothfuchs T, Sanden T, Sineriz J L, Sugita Y, Svemar C, Thomas H, 2005. Full-Scale Testing of the KBS-3V Concept for the Geological Disposal of High-Level Radioactive Waste: PROTOTYPE REPOSITORY. Final Report. Nuclear science and technology.
- Booker J R, Savvidou C, 1985. Consolidation around a point heat source. *Int. J. Numer. Anal. Methods Geomech* 9(2): 173-184.
- Börgesson L, Fredrikson A, Johannesson L-E, 1994. Heat conductivity of buffer materials. SKB TR-94-29, Svensk Kärnbränslehantering AB.
- De Bruyn D, Labat S, 2002. The second phase of ATLAS: the continuation of a running THM test in HADES underground research facility at Mol. *Engineering Geology* 2002; 64(2-3): 309-16
- ENRESA, 2000. FEBEX project. Full-scale engineered barriers experiment for a deep geological repository for high level radioactive waste in crystalline host rock. Final Report. Publication. Tecnica ENRESA 1/2000, Madrid, 354 pp.
- Ferrari A, Laloui L, 2012. Advances in the testing of the hydro-mechanical behaviour of shales. Laloui L, and Ferrari A., (eds). *Multiphysical Testing of Soils and Shales*, pages 57 - 68, Springer
- Gaus I, Wiczorek K, Schuster K, Garitte B, Senger R, Vasconcelos R, Mayor J C, 2014. EBS behaviour immediately after repository closure in a clay host rock: HE-E experiment (Mont Terri URL). *Geol. Soc. London, Spec. Publ.* 400, 71–91.
- Ghabezloo S, 2010. Effect of porosity on the thermal expansion coefficient: A discussion on the paper 'Effects of mineral admixtures on the thermal expansion properties of hardened cement paste' by Z.H. Shui, R. Zhang, W. Chen, D. Xuan, *Constr. Build. Mater.* 24 (9) (2010) 1761–1767. *Construction and Building Materials* 2010; 24(9): 1796–8.
- Hudson J A, Jing L, 2013. Demonstration of coupled models and their validation against experiment: The current phase DECOVALEX 2015. 392-396. Feng X T, Hudson J A, Tan F (eds): *Rock Characterisation Modelling and Engineering Design Methods*. (published by) CRC Press/Balkermam Leiden, Netherland.
- Huertas F, Fuentes-Cantillana J L, Jullien F, Rivas P, Linares J, Farina P, Ghoreychi M, Jockwer, N, Kickmaler W, Martinez M A, Samper J, Alonso E, Elorza F J, 2000. Full-Scale Engineered Barriers Experiment for a Deep Geological Repository for High-Level Waste in Crystalline Host Rock – Phase II FEBEX II. Final Report. Publication. Tecnica ENRESA 1/2000, Madrid, 354 pp.
- Jacinto A C, Villar M V, Gomez-Espina R, Ledesma A, 2009. Adaption of the van Genuchten expression to the effects of temperature and density of compacted bentonites. *Applied Clay Science* 42 (2009) 575-582.
- Johnson L H, Niemeyer M, Klubertanz G, Siegel P, Gribi P, 2002. Calculations of the temperature evolution of a repository for spent fuel, vitrified high-level waste and intermediate level waste in Opalinus Clay. Nagra Technical Report NTB 01-04. Nagra, Wettingen, Switzerland.
- Kahr G, Müller-Vonmoos M, 1982. Wärmeleitfähigkeit von bentonit MX80 und von Montigel nach der heizdraht methode. Technical report, Nagra. NTB 82-06.

- Kolditz O, Görke U J, Shao H, Wang W (eds) 2012. Thermo-hydro-mechanical-chemical processes in Fractured porous media. Springer, Heidelberg.
- Kozeny J, 1927. Ueber kapillare Leitung des Wassers im Boden. Sitzungsbeber Akad. Wiss; 1927, 136(2a): 271–306.
- Lewis R W, Schrefler B A, 1998. The finite element method in the static and dynamic deformation and consolidation of porous media, 2nd edition: 57-65. Chichester: John Wiley & Sons Ltd.
- Li M, Xiao W L, Guo X, Zhang L H, Zheng L L, 2009 Laboratory study of the effective pressure law for permeability of the low-permeability sandstones from the Tabamiao area, Inner Mongolia. Chinese Journal of Geophysics 2009; 52(6): 1402–13.
- Martin C D, Lanyon G W, 2003. Measurement of in situ stress in weak rocks at Mont Terri Rock laboratory, Switzerland. Int. J. Rock Mech. Mining Sci. 40, Nos 7-8, 1077-1088
- Müller H R, Weber H P, Köhler S, Vogt T, 2012. The full-scale Emplacement (FE) Experiment at the Mont Terri URL. Clay in natural and engineered barriers for radioactive waste confinement- 5 International meeting Book for abstracts, (p. 923) France.
- Olivella S, Carrera J, Gens A, Alonso E E, 1994. Non-isothermal multiphase flow of brine and gas through saline media. Trans. Porous Media 15(3): 271-293.
- Rizzi M., Laloui L, P. Marschall, 2010. “Granular MX-80 Bentonite as Buffer Material: a Focus on Swelling Characteristics”. of the material Mechanics. Proceedings of the 1st EDCM2010 on Advances in Modern Aspects of Mechanics Lausanne, Switzerland.
- Romero E, Gómez R, 2013. Water and air permeability tests on deep core samples from Schlattingen SLA-1 borehole. Nagra-Arbeitsbericht NAB 13-51. Nagra, Wettingen, Switzerland.
- Rutqvist J, Börgesson L, Chijimatsu M, Kobayashi A, Nguyen T S, Jing L, Noorishad J, Tsang C F, 2001. Thermohydrmechanics of partially saturated geological media-governing equations and formulation of four finite element models. Int J Rock Mech Min Sci 38: 429-442.
- Stephansson O, Hudson A, Jing L (eds), 2004. Coupled thermo-hydro-mechanical-chemical processes in geo-systems: fundamentals, modelling experiments and applications. Elsevier, Oxford, 831.
- Tang A M, Cui Y J, 2010. Effects of mineralogy on thermo-hydro-mechanical parameters of MX80 bentonite. Journal of Rock Mechanics and Geotechnical Engineering 2 (1): 91–96
- Teodori S.P, Gaus I, (Eds.) 2011. Long Term Performance of Engineered Barrier Systems (PEBS). Mont Terri HE-E experiment: as built report. Nagra Arbeitsbericht NAB 11-25. Nagra, Wettingen, 125 pp.
- Villar M V, 2002. Thermo-hydro-mechanical characterization of a bentonite from Cabo de Gata. A study applied to the use of bentonite as sealing material in high level radioactive waste repositories. ENRESA publicación técnica 04/2002. Madrid.
- Villar M V, 2012. THM cells for the HE-E test: setup and first results. PEBS Reports D2.2.7a-VER.0. CIEMAT Technical Report CIEMAT/DMA/2G210/03/2012
- Villar M V, Martin P L, Romero F J, 2014. Long-term THM tests reports: THM cells for the HE-E test: update of results until February 2014. CIEMAT Technical Report CIEMAT/DMA/2G210/03/2014

- Walls J D, 1982. Effects of Pore pressure, confining pressure and partial saturation on permeability of sandstones. PhD Thesis. Stanford, USA: Stanford University.
- Wang W Q, Rutqvist J, Görke U J, Birkholzer J T, Kolditz O, 2011. Non-isothermal flow in low permeable porous media: a comparison of Richards' and two-phase flow approaches. *Environ Earth Sci* 62 (2011), 1197-1207.
- Wermeille S, Bossart P, 1999. In situ stress in Mont Terri region: Data compilation, Technical Report 99-02. Mont Terri Project.
- Wieczorek K, Mieke R, Garitte B. 2011. Measurement of Thermal properties of the HE-E Buffer materials. PEBS Deliverable D2.2-5.
- Wieczorek K, Mieke R, Garitte B. 2013. Thermal characterisation of the HE-E Buffer. PEBS Deliverable D2.2-9.
- Wileveau Y. THM behaviour of host rock: (HE-D) experiment: progress report. Part 1. Technical Report TR 2005-03, 2005.
- Wileveau Y, Su K. In situ thermal experiment carried out in Opalinus Clay and Callovo-Oxfordian claystones by Andra—experiment set-up and measurement results. ANDRA report. Paris, France, 2007.
- Xu W J, Shao H, Hesser J, Wang W Q, Kolditz O, Popp T, 2011. Simulation of dilatancy-controlled gas migration process in saturated argillaceous rock. In: *Proceeding of the 2nd International Symposium on Computational Geomechanics: COMGEO II*. Rhodes: International Centre for Computational Engineering, 2011: 693–703.
- Xu W J, Shao H, Marschall P, Hesser J, Kolditz O, 2013. Analysis of flow path around the sealing section HG-A experiment in the Mont Terri Rock Laboratory. *Environ. Environmental Earth Sciences* 2013; 70(7): 3363–80.
- Zhang C L, Czaikowski O, Rothfuchs T, 2010. Thermal-hydro-mechanical behaviour of the Callovo-Oxfordian clay rock. Final report of GRS. 2010: 121–36.
- Zhang C L, Wieczorek K, Rothfuchs T, Armand G, Lebon P, 2009. Responses of the Opalinus Clay to heating during the HE-D experiment at Mont Terri. In: *Proceedings of the European Commission TIMODAZ-THERSA International Conference*. Luxembourg, 2009.
- Åkesson M, Börgesson L, Kristensson O, 2010. THM modelling of buffer, backfill and other system components, SR-Site Data report, Technical Report TR-10-44: 49-58

List of associated publications

First author publications peer-reviewed international journals

[EP1] **Wang X. R.**, Shao H., Hesser J., Zhang C. L., Wang W. Q., Kolditz O., (2014): Numerical analysis of thermal impact on hydro-mechanical properties of clay. *Journal of Rock Mechanics and Geotechnical Engineering*. 10/2014 6(5): 405-416, doi: 10.1016/j.jrmge.2014.07.002. (listed in SCOPUS)

[EP2] **Wang X. R.**, Shao H., Wang W. Q., Hesser J., Kolditz O., (2015): Numerical modeling of heating and hydration experiments on bentonite pellets. *Engineering Geology* 198 (2015) 94-106, doi:10.1016/j.enggeo.2015.09.009. (ISI listed)

[EP3] **Wang X. R.**, Shao H., Hesser J., Kolditz O., (2016): Analysis of the THM behaviour in a clay-based engineered barrier system (EBS): modelling of the HE-E experiment (Mont Terri URL). *Environ Earth Sci* (2016)75:1350, doi: 10.1007/s12665-016-6116-1. (ISI listed)

Other publications

Wang X. R., Shao H., Hesser J., Zhang C. L., Wang W. Q., Kolditz O., (2015): Numerical analysis of laboratory heating experiment on clay-based material. *Proceedings ISRM REGIONAL SYMPOSIUM EUROCK 2015*. Oct. 2015, Salzburg, Austria

Shao H., Paul B., **Wang X. R.**, Müller H. R., (2015): Near-field permeability distribution of FE tunnel in the Mont Terri Rock Laboratory: Influence of shotcrete lining on EDZ development. *Conference paper: Clay Conference 2015*, March 2015, Brussel, Belgium

Garitte B., Lee C., Maekawa K., Manepally C., Pan P., Rutqvist J., Graupner B., **Wang X. R.**, Shao H., Nguyen S. (2015): DECOVALEX-2015: A THM modelling benchmark based on the performance of heated and hydrated granulated bentonite mixture column tests. *Conference paper: Clay Conference 2015*, March 2015, Brussel, Belgium

Book chapter

Wang X. R., Hesser J., (2015): Chapter 4.2: Undrained heating. In book: Kolditz O., Shao H, Wang W. Q., Bauer S., (eds): *Thermo-Hydro-Mechanical-Chemical Processes in Fractured Porous Media: Modelling and Benchmarking*. Publisher: Springer. PP: 124-130. ISSN: 2363-6181. doi: 10.1007/978-3-318-11894-9

Theses

1. The high temperature can induce a strong variation in water saturation that can in turn cause a change in the thermal conductivity of the porous medium. The relations between the thermal conductivity of the bentonite buffer and the water saturation were intensively studied based on numerous measurements. Thereby the water-saturation-dependent thermal conductivity was developed.
2. Many measurements have indicated that the high temperature can reduce the water-retention capacity. Based on the measured water-retention behaviour in this work, the van Genuchten function was modified to take into account the temperature effects. The modified van Genuchten function has been applied to describe the water retention behaviour of MX80 bentonite in the modelling of the column test, which leads to a better agreement between the calculated and measured relative humidities, especially at high temperature.
3. The increase of temperature could induce a strong pore-pressure response in a saturated clay formation, which could change the structure of the pore space and thereby change the permeability. In this work, a pore-pressure-controlled permeability model was developed and applied in the modelling of a heating test on the Callovo-Oxfordian clay (COX). The results indicated that the evolution of pore pressure at the high temperature level can be reproduced only when the pore-pressure-induced change in permeability is considered.
4. The strong anisotropic properties of the clay rock due to the presence of bedding are considered in the model by using the bedding-orientation-dependent thermal conductivities, anisotropic permeability tensor, and transversely isotropic mechanical parameters. Besides, the swelling/shrinkage behaviours were assumed to be anisotropic. Therefore an anisotropic swelling/shrinkage model was developed that is dependent on the change of water saturation and the bedding orientation. With the anisotropic swelling/shrinkage model, the different behaviours between the radial and axial strains during the heating experiment on COX can be interpreted well.
5. In the modelling of the heating experiment on COX, the effects of the presence of gas in the pore space on the pore pressure evolution were numerically analysed. A more intensive thermally induced pore-pressure response was observed when the gas effects were not considered.
6. The storage capacity of one porous medium that is related to the porosity and compressibility of the solid and the pore fluid is very difficult to measure. In the HE-E modelling, the storage capacity is estimated to have a significant effect on the thermally induced pore-pressure response.
7. Generally the rate of the resaturation process in the repository is determined by the permeability of both the host rock and the buffer material. In the long-term modelling of the HE-E test, the threshold value of buffer permeability, from which the rate of water intake into the EBS is governed by the permeability of the host rock, was analysed by performing calculations of the variation of different saturated water permeabilities of the buffer material.

Thesen

1. Die hohe Temperatur kann eine starke Veränderung der Wassersättigung verursachen, die wiederum die Wärmeleitfähigkeit vom porösen Medium ändern kann. Die Abhängigkeit der Wärmeleitfähigkeit des Bentonits von der Wassersättigung wurde anhand einer Vielzahl von gemessenen Daten intensiv untersucht. Dadurch wurde eine wassersättigungsabhängige Wärmeleitfähigkeit entwickelt.
2. Viele Messergebnisse haben gezeigt, dass die hohe Temperatur das Wasserrückhaltevermögen verringern kann. In dieser Arbeit wurde die van Genuchten Funktion auf Basis der gemessenen Daten modifiziert um die Temperatur Effekte zu berücksichtigen. Die modifizierte van Genuchten Funktion wurde zur Beschreibung der Wasserrückhalte von Bentonit in der Modellierung der Langzeit-Heiz- und Aufsättigungs-Experiment verwendet, dass zu einer besser Übereinstimmung von der berechneten und der gemessenen relativen Feuchtigkeit insbesondere bei hoher Temperatur führte.
3. Die Anstieg der Temperatur kann eine starke Poren Druck Reaktion in der gesättigten Tonsteine induzieren, die die Porenstruktur ändern würde. Hiermit würde die Permeabilität verändert. Zur Beschreibung diese Effekte wurde ein poredruckabhängiges Permeabilitätsmodell entwickelt und in die Modellierung der Heiz Experiment für Callovo-Oxfordian Clay (COX) verwendet. Die Modellierungsergebnisse zeigten, dass die gemessene Entwicklung des Poredrucks bei hohe Temperatur im Modell nur unter Berücksichtigung der poredruckinduzierten Veränderung von Permeabilität nachvollziehen kann.
4. Die stark anisotropen Eigenschaften von Tonsteinen werden im Modell durch die Definition von unterschiedlichen Werten für die Wärmeleitfähigkeit parallel und senkrecht zur Schichtung, dem transversal isotropen Permeabilitätstensor, der transversal isotropen mechanischen Parametern berücksichtigt. Außerdem wurde ein von Schichtungsorientierung abhängiges anisotropes Quell- und Schrumpfmotiv entwickelt. Die Anwendung des anisotropen Quell- und Schrumpfmotiv kann die in das Heiz Experiment für COX beobachteten unterschiedlichen Verhalten zwischen der axialen und radialen Verzerrung gut interpretiert.
5. In der Modellierung des Laborversuchs des Callovo-Oxfordian Tons wurden die Einflüsse von Porengas auf die Poredruckentwicklung numerisch analysiert. Eine schnelle und intensive Poredruck Reaktion wurde berechnet, wenn die Gas Effekte nicht berücksichtigt war.
6. Die Speicherkapazität von porösen Medien, die von der Porosität, der Kompressibilität des Feststoffs und dem Porenfluid abhängig ist, ist sehr schwierig zu messen. Durch die HE-E Modellierung wurde abgeschätzt, dass die Speicherkapazität eine wichtige Rolle in der thermisch induzierten hydraulischen Reaktion spielt.
7. Generell, die Geschwindigkeit der wieder Sättigungsprozess ist von der Permeabilität der Wirtsgesteine und der Puffermaterial zusammen entschieden. In die langzeitige Modellierung wurden die Permeabilitätsschwellenwerte der Puffermaterialien mit Hilfe von Variationsberechnungen mit unterschiedlichen wassergesättigten Permeabilitäten für die Puffermaterialien untersucht. Dabei wurde festgestellt, ab welcher Permeabilität von der Puffermaterialien die Rate der Wasserzufuhr in das EBS im Wesentlichen durch die Permeabilität des Wirtsgesteins bestimmt wird.